AN INVESTIGATION OF THE CRYSTAL STRUCTURES OF α AND β-$Cu_2P_2O_7$

AN INVESTIGATION OF THE CRYSTAL STRUCTURES OF α AND β-$Cu_2P_2O_7$

By

BEVERLY ELLIS ROBERTSON, B.Sc.

A Thesis

Submitted to the Faculty of Graduate Studies

in Partial Fulfilment of the Requirements

for the Degree

Master of Science

McMaster University

May 1965

MASTER OF SCIENCE (1965)
(Physics)

McMaster University
Hamilton, Ontario

TITLE: An Investigation of the Crystal Structures of α and β-$Cu_2P_2O_7$.

AUTHOR: Beverly Ellis Robertson, B.Sc. (University of New Brunswick)

SUPERVISOR: Professor C. Calvo

NUMBER OF PAGES:

SCOPE AND CONTENTS:

A high temperature polymorph of α-$Cu_2P_2O_7$ was found above 70°C. The lattice parameters and space groups of both phases were determined from X-ray photographs. The crystal structures of α and β-$Cu_2P_2O_7$ were refined by crystallographic least squares analysis and the molecular geometry obtained was compared with that of other closely related compounds of the transition metal ion pyrophosphate series. The central oxygen atom was found to have enhanced thermal motion or disorder in agreement with I.R. spectroscopic studies of Lazarev. The bond lengths obtained for the $P_2O_7^{4-}$ ion were discussed in reference to values predicted by Cruickshank. Evidence of a Jahn-Teller effect was found in the case of the Cu^{++} ion. A description is given of a relatively efficient method of measuring intensities of Bragg reflections, using a single crystal diffractometer.

ACKNOWLEDGEMENTS

I should like to express my sincere gratitude to Professor C. Calvo for his guidance and help throughout the course of this research. Thanks are also extended to Professor I. D. Brown for helpful discussions and to Casimir Rosa for his assistance in the translation of some of the pertinent literature.

I wish to acknowledge the receipt of a National Research Council bursary, a McMaster University graduate scholarship and an Ontario Government Fellowship. This research was made possible through grants-in-aid from the National Research Council to Professor C. Calvo.

TABLE OF CONTENTS

LIST OF TABLES

LIST OF ILLUSTRATIONS

CHAPTER 1: INTRODUCTION

This study is one of a series directed towards obtaining an understanding of the crystal chemistry of pyrocompounds. In particular, the divalent ion pyrophosphates have been chosen for initial study since they manifest a broad range of behaviour but with sufficient crystallographic similarity to make a comparison meaningful. These pyrophosphates, defined as $2MO:P_2O_5$ (M = metal), fall roughly into two classes, the "alkaline earth" pyrophosphates and the "transition metal ion" pyrophosphates. $Mg_2P_2O_7$ is an anomally in this nomenclature since its behaviour places it in the "transition metal ion" group. However, in this thesis $Mg_2P_2O_7$ will be classed with the "transition metal ion" pyrophosphates notwithstanding the fact that magnesium is generally regarded as an alkaline earth metal.

The luminescent properties of the alkaline earth group, consisting of $Ba_2P_2O_7$, $Ca_2P_2O_7$ and $Sr_2P_2O_7$, were studied by Ranby, Mash and Henderson (1951). They used Sn^{++} as the primary activator and Mn^{++} as the secondary activator in $(M_X, R_{1-X})_2P_2O_7$; (M, R = Cu, Ba, Sr; $0 \leq X \leq 1$) with X and the Mn^{++} concentration as variables. Changes were found in both the luminescent wavelength and intensity and some of these changes correspond to the appearance of polymorphic phases.

The correlation among these phases and their transition temperatures is illustrated in Figure 1. $Ca_2P_2O_7$ has three stable phases above room temperature. The low temperature form (γ) is stable below 750°C. The intermediate phase (β) is stable between 750°C and 1150°C. A third form (α) is found when the compound is fired above 1150°C and persists up to the melting point of 1230°C. The phase behaviour of $Sr_2P_2O_7$ is similar to that of $Ca_2P_2O_7$ except for the fact that a γ form has not been found. Here, the β and α transition occurs at 750°C. On the other hand $Ba_2P_2O_7$ has no γ or β form but it has a unique phase δ which appears when the compound is fired above 790°C.

No crystallographic studies beyond the recording of their powder pattern have been made of either γ-$Ca_2P_2O_7$ or δ-$Ba_2P_2O_7$. The α forms appear to be isomorphic, as do the β forms of $Ca_2P_2O_7$ and $Sr_2P_2O_7$. Ranby et. al. determined the lattice parameters of the α forms of these compounds from single crystal photographs and have shown them to be members of the orthorhombic crystal system. Corbridge (1957) investigated single crystals of β-$Ca_2P_2O_7$ and found them to be members of the tetragonal space group P_{41}. The powder pattern of β-$Sr_2P_2O_7$ has been studied by Hoffman and Mooney (1960) and because of the similarities of its powder pattern to that of β-$Ca_2P_2O_7$, they assume that β-$Sr_2P_2O_7$ also crystallizes in space group P_{41}. The lattice parameters together with their symmetries,

where known, are given in Table 1. Unfortunately the structures of none of the alkaline earth pyrophosphate phases have as yet been determined.

The luminescent behaviour and other physical properties of the alkaline earth pyrophosphates show discontinuities across the phase transitions. The transformations were very "sluggish" and thus the high temperature forms of the crystals could be obtained as metastable phases at room temperature. This suggests that the atomic displacements that transform one phase to another are not small and may involve bond rearrangement.

The compounds known to be among the "transition metal ion" pyrophosphates are those of Mn^{++}, Cu^{++}, Mg^{++}, and Zn^{++}. A fair amount of data has been obtained on the"transition metal ion" pyrophosphates since this present research was begun. The high temperature forms (β) appear to be isostructural. Each compound except $Mn_2P_2O_7$ shows a low temperature polymorph (α)*. The differential thermal analysis curves of $Mg_2P_2O_7$ and $Zn_2P_2O_7$ were investigated by Roy, Middlesworth and Hummel (1948) and Katnack and Hummel (1957) respectively. $Mg_2P_2O_7$ and $Zn_2P_2O_7$ undergo endothermic transitions near 68°C and at 132°C respectively. The crystal structures of β-$Mg_2P_2O_7$ and $Mn_2P_2O_7$ have been studied by Lukaszewicz (1961) and Lukaszewicz and Smajkiewicz (1961). Although the atomic co-ordinates

* For historic reasons the convention of using the Greek letter α to label the low temperature form of the"transition metal ion" pyrophosphates is a reversal of the convention used to label the alkaline earth pyrophosphates.

had not been well refined, the atomic geometry is isostructural to that of thortvetite ($Sc_2Si_2O_7$) as reported by Zachariasen (1930). The crystal structure of β-$Zn_2P_2O_7$ (Calvo, 1965) has also been shown to be isomorphic to the other members of the series.

A common difficulty exists in the case of the high temperature structures in that the space group ambiguity resists easy resolution. The symmetry of the diffracted X-rays, together with the extinguished reflections, limits the space group to one among Cm, C_2, or C 2/m. The importance of the proper space group determination is magnified by the fact that the anion must be linear in the C 2/m space group and would apparently provide direct evidence for the existence of this controversial chemical entity.

Zachariasen chose C 2/m, the only centrosymmetric possibility as the space group for thortveitite. More recent work by Cruickshank, Lynton and Barclay (1962) has supported this choice. The agreement between observed and calculated structure factors for structures refined in each of these space groups was about equal and since the agreement can always be improved by the inclusion of more variable parameters it was concluded that this was evidence in favour of the centrosymmetric space group. Further the discrepancy between chemically equivalent bonds in the anion was unreasonable in the structure refined in Cm and unfavourable although not clearly unreasonable in C 2. In total it was considered that the space group was most probably

C 2/m although the evidence can not be regarded as conclusive. The same space group ambiguities exist for the high temperature forms of the "transition metal ion" series.

The same space group ambiguities exist for other members of the series. In the case of the An and Mg pyrophosphates, the crystallographic choice of C 2/m has been confirmed by electron spin resonance studies. (Chambers, Datar, Calvo (1964) and Leung Jurn Sun (1964)). In these β phases only one site is seen for the paramagnetic ion and this is consistent only with the higher symmetry, C 2/m. In addition the space group of $Mn_2P_2O_7$ has been shown to be C 2/m by the use of the anomalous dispersion of Mn^{++} for CoKα radiation (Calvo, private communication). The unit cell data for these phases is summarized in Table 3. Included in the table are data on $Cu_2P_2O_7$ which will be discussed later.

All the transitions appear reversible, which implies only small structural differences between the various phases common to a given compound. In the case of $Zn_2P_2O_7$, the intermediate phase was first detected by esr techniques. In addition, these results suggested that the crystal transformed from space group symmetry C m to C 2/m around 155°C and that this transition was gradual in temperature. In $Mg_2P_2O_7$, early X-ray powder patterns also seemed to indicate the co-existence of two phases over an extended temperature region, as did the specific heat measurement (Oetting and McDonald (1963)). These experiments substantiate those of Roy et. al. (1948). Recent esr experiments on $Mg_2P_2O_7:Mn^{++}$ may be

interpreted in terms of two phases co-existing over a much narrower temperature range of $2^{o}C$. However, single crystal experiments indicate that the co-existence would not be between the α and β phases, but between β and some new phase. This question of gradual phase transitions is one that has only recently been receiving any substantial experimental investigation.

The geometry of the pyrophosphate ion could be of importance in understanding the chemistry of the covalent bond in inorganic systems. The geometric configuration assumed by a structural group, such as the $P_2O_7^{-4}$ ion, is in part determined by the strengths of the bonds within the ion. If the interatomic distances and/or the angles are varied, the character of the bonds will change. The actual configuration adopted in a crystalline environment will be a compromise between the maximum stability of the anion and reasonable packing of these anions with the cations to form a translationally symmetric three dimensional crystal.

The bond lengths and angles found for the anion in a given crystal provide a measure of the bond strengths and character. The strength is generally approximated by the overlap integral of the wave function of the bonding electrons between adjacent atoms forming the bond. Further, one assumes a functional relationship between the bond distance and character determined from the L.C.A.O. corresponding to the proper symmetry for the anion and the magnitude of the overlap

integral independent of the character of the electrons "shared". Therefore, by imposing small changes in a basic structure as for example by changing the cation or changing the phase and studying the resultant crystalline geometry, one can gain some understanding of the relative importance of various factors in determining the chemical bonding. Because of the near isomorphism of the various phases and compounds, the"transition metal ion" pyrophosphates are in ideal system for study in this regard.

In detail, the $P_2O_7^{4-}$ ion can be regarded as two PO_4^{-3} tetrahedra joined across a common oxygen atom (to be referred to as the central oxygen atom) as in Figure 2. The relative angle of these tetrahedra and the size of the inner and outer P-O bond distances are regarded as perturbations on the basic PO_4^{-3} structure.

Cruickshank (1961) has discussed the nature of the P-O bonds in PO_4^{3-} tetrahedra and $P_2O_7^{4-}$ groups. After the sp^3 σ bonds are constructed, two π bonding systems are formed from the phosphorus dY orbitals and the oxygen $2p\pi$ orbitals. A σ lone pair is left at the back of each oxygen atom, which may bond with other atoms in a solid phase.

The way in which the π orbitals extend across the central oxygen atom is dependent on the P-O-P angle between the tetrahedral pair. At a P-O-P bond angle of $109^{\circ}25'$ the bonding electrons of the central oxygen atom are sp^3 hybridized permitting only two

bonds to be formed from the tetrahedrally disposed orbitals with no π bonds running throughout the molecule. In the case of sp^2 hybridization, only one π system joins across the central oxygen and sp hybridization corresponds to a linear P-O-P group with both π systems joining across the central oxygen atoms. Thus, as the angle approaches 180°, the P-O(P) distance should become shorter. Cruickshank has given a curve of observed bond length versus bond order determined from valence bond theory. As a first approximation this curve is assumed to be linear. Bond orders and predicted bond lengths based on these considerations for the P-O(P) and P-O bonds are listed in Table 2. Only the linear and sp^2 cases are considered. It should be noted that these predictions ignore the effect of environment on the $P_2O_7^{4-}$ ion.

Lukaszewicz and Nagler (1961) have investigated the powder pattern of $Cu_2P_2O_7$ at room temperature. They prepared crystals by adding $Na_2P_2O_7$ to Cu_2SO_4 and heating the precipitate to $1140^\circ C$ either on a platinum plate or in a corundum boat. Monoclinic crystals were obtained. The lattice parameters derived from their powder pattern are given in Table 4 where they are compared to the values to be reported here. From the extinctions in the X-ray pattern, either the space group C 2/c or C c is allowed. They predicted that α-$Cu_2P_2O_7$ had a structural similarity to the high temperature form of the other transition metal ion pyrophosphates but with the c lattice

parameter doubled. This suggested that a high temperature form with space group C 2/m might exist in analogy with the other members of the series. Roy, Middlesworth and Hummel (1948) reported some indication of a phase change in the differential thermal analysis curve for $Cu_2P_2O_7$.

In summary, the study of the crystallography of the pyrophosphates is undertaken in order to understand what parameters are important in determining the subtle differences in the many phases of the"transition-metal ion" family of compounds. In addition we hope to pursue questions regarding the geometry of the anion. Lastly a knowledge of the accurate atomic parameters are necessary in order to investigate the validity of various proposed theories relating the zero field splitting parameter of Mn^{++} to the tetragonal component of the electric field. (Chambers, thesis) Measurements by esr techniques of this splitting parameter, D, are under current investigation.

TABLE 1

Crystallography of Alkaline Earth Pyrophospates

	a(A)	b(A)	c(A)	Crystal Systems and Space Group
α-$Ca_2P_2O_7$	8.44	12.52	5.26	(orthorhombic)
α-$Sr_2P_2O_7$	8.87	13.27	5.39	(orthorhombic)
α-$Ba_2P_2O_7$	9.35	13.87	5.61	(orthorhombic)
β-$Ca_2P_2O_7$	6.66		23.86	(tetragonal, P_{41})
β-$Sr_2P_2O_7$	6.92		24.79	(tetragonal, P_{41})

TABLE 2

Predicted Lengths of P-O Bonds*

P-O-P Angle	Bond	Bond Order	Bond Length (A)
120°	P-O	1 3/5	1.51
120°	P-O(P)	1 1/5	1.64
180°	P-O	1 8/15	1.53
180°	P-O(P)	1 2/5	1.58

* Cruickshank (1961)

TABLE 3

Crystallography and Phase Relations of the Transmission Metal Ion Pyrophosphates

	a(A)	b(A)	c(A)	β	Z	Space Group	Range of Stability
β-$Zn_2P_2O_7$	6.61	8.29	4.51	105.4°	4	C 2/m	above 155°C
β'-$Zn_2P_2O_7$	6.61	8.29	4.51	105.4°	4	C m	132°C - 155°C
α-$Zn_2P_2O_7$	19.83	8.29	9.02	105.4°	24	I c	below 132°C
β-$Mg_2P_2O_7$	6.494	8.28	4.522	103.8°	4	C 2/m	above 68°C
β'-$Mg_2P_2O_7$	?	8.28	?	103.8°		?	63 - 65°
α-$Mg_2P_2O_7$	12.98	8.28	9.04	103.8°	16	B 2_1/c	below 68°C
β-$Cu_2P_2O_7$	6.827	8.118	4.567	108.85°	4	C 2/m	above 70°C
α-$Cu_2P_2O_7$	6.877	8.113	9.162	109.54°	8	C 2/c	below 70°C
$Mn_2P_2O_7$	6.63	8.58	4.54	102.66°	4	C 2/m	at least -60°C

Fig.1

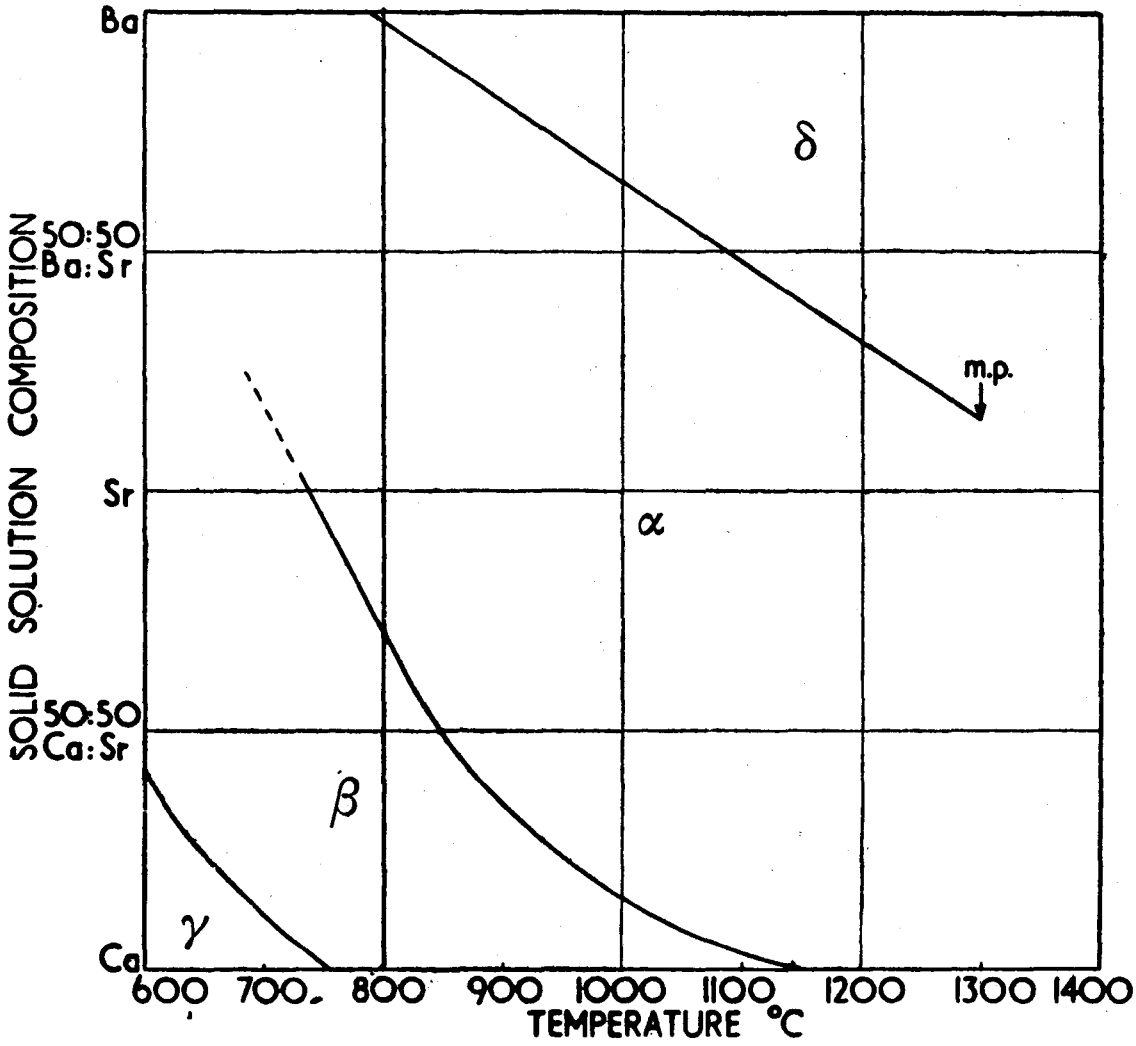

Approximate phase diagram for pure (ALKALINE EARTH) pyrophosphates

From Ranby et. al. (1955)

Geometry of the Pyrophosphate Group

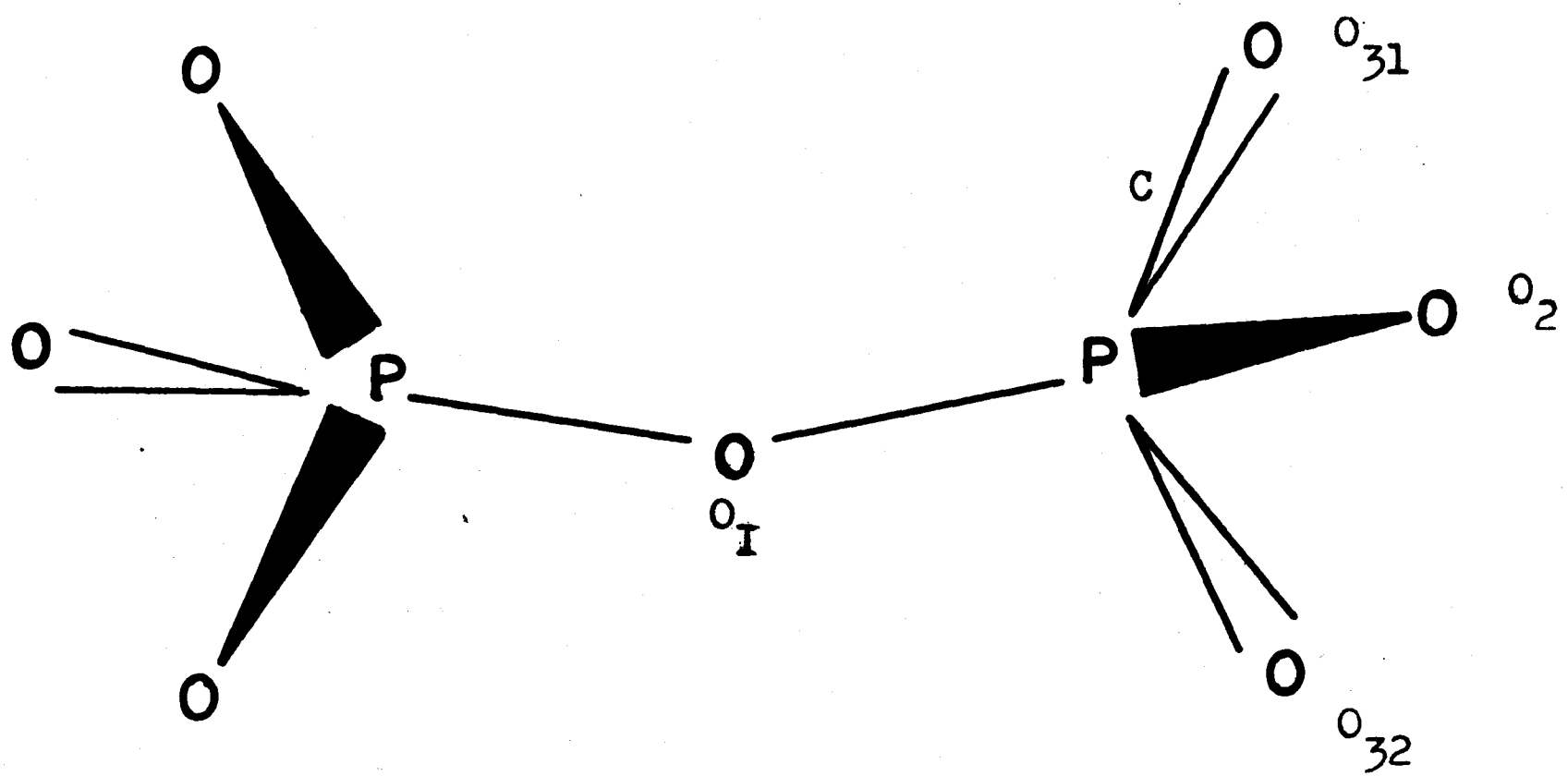

Fig.2

CHAPTER 2: THE PHASE TRANSITION IN $Cu_2P_2O_7$

First we wanted to investigate the structure of the high temperature phase. An attempt was made to find the transition temperature, using relatively crude differential thermal analysis apparatus (Daniels et. al. (1956)). The $Cu_2P_2O_7$ was prepared by a procedure analogous to that of Lukaszewicz and Nagler but the crystals were grown in an open vycor tube. Small blue green crystals were obtained. These were ground to a powder and placed in one side of the brass sample holder. A standard ZnO powder was placed in the other side. Chromel-Alumel thermocouples placed in each sample were connected in opposition so that only when the temperatures of the two samples differed would an emf be developed. The temperature of the brass block was determined from emf readings of a third chromel-alumel thermocouple. The sample was heated at a rate of $0.5^{\circ}C/min.$ and ΔT and T measurements were taken periodically. The resulting ΔT versus T plot was inconclusive although both the heating and cooling curves seemed to show a small endothermic peak at $180 \pm 6^{\circ}C$. It was tentatively assumed that the peak corresponded to the phase change we were seeking.

Consequently an attempt was made to confirm the transition with X-rays. A crystal was glued to a glass fibre with Stycast 2651 High Temperature Cement. The fibre was affixed to a brass pin with Stycast cement and the pin was mounted on a goniometer. The crystal was heated by means of a hot soldering iron placed approximately 1.5 mm from the crystal. The temperature of the soldering tip was controlled by passing the current through a powerstat and the system was calibrated by substituting a chromel-alumel thermocouple in place of the crystal. The temperature was recorded for several settings of the powerstat and the separation between the crystal and the heating element. Because of the high sensitivity of the crystal temperature to this separation and the fact that this distance could not be measured accurately, the temperatures reported for the crystals have an error of about $10^{\circ}C$.

The crystal was approximately aligned optically using reflections from the crystalline faces such that the c axis of the crystal coincided with the axis of rotation of the spindle of a Weissenberg camera. Final corrections to the alignment were made from oscillation photographs with the crystal heated to $200 \pm 10^{\circ}C$. The alternate layer lines had disappeared at the temperature, indicating the existence of a high temperature polymorph with the c axis halved. Also the glue had allowed the crystal to relax and the crystal had to be realigned. Subsequently the crystal's orientation did not change.

Consequently, for all following experiments the crystal was heated for at least two hours before final alignment was carried out.

A zero layer line Weissenberg photograph (Buerger (1942)) was taken at room temperature. The crystal was reheated to 200°C and another photograph was taken. The photographs were identical except for small changes in the shape and the intensity of the reflections. In both cases, reflections for which $h + k = 2n + 1$ (where n is an integer) did not appear. A smaller crystal was aligned about the b axis. Zero layer line Weissenberg photographs were taken at both temperatures. The reflections with odd values of ℓ (indexed with respect to the α-$Cu_2P_2O_7$ unit cell) did not appear at high temperatures. Also spots with k = zero and ℓ odd did not appear at room temperature. This limits the low temperature form to space groups C 2/c or C c and the high temperature form to C 2, C m or C 2/m, but with the unit cell doubled in the c direction in the case of the low temperature form. Weissenberg photographs obtained with CuKα radiation were taken for the purpose of intensity measurements (to be described later).

These experiments did not determine the temperature at which the transition occurs, but only that the phase at 200°C is different from that at room temperature. Therefore, a crystal was mounted onto the tip of a thermocouple with Stycast cement. The thermocouple

leads were passed through a two-hole ceramic insulating rod around which a heating coil of nichrome wire was wound. The current for the heater was controlled by two powerstats connected in series. Ten minute oscillation photographs were taken about the c axis at temperatures ranging from 25°C to 200°C. An exposure at 64 ± 4°C contained additional reflections corresponding to the first layer lines of the α phase. At 74° ± 2°C these spots were not present. Therefore, the transition appears to occur at 70° ± 4°C.

CHAPTER 3: DETERMINATION OF LATTICE PARAMETERS

The lattice parameters given by Lukaszewicz and Nagler for α-$Cu_2P_2O_7$ were used during most of the earlier work. The c axis of β-$Cu_2P_2O_7$ was taken to be one-half the α-$Cu_2P_2O_7$ c axis. It was necessary, however, to verify these results and to obtain accurate high temperature parameters.

A crystal was mounted with the b axis, along the goniometer axis. Two Weissenberg photographs were superimposed, one with the crystal at room temperature, and one at 100°C with the camera displaced to prevent superpositioning of reflections. A TiO_2 powder photograph was taken through the Weissenberg screen and superimposed at both ends of the previous photographs. Corrections to the effective camera radius as a function of Θ were plotted, based on the positions of the TiO_2 lines and its accurately known cell parameters of a = 4.5929A and c = 2.9591A (Baur (1959)). The Θ values for α and β-$Cu_2P_2O_7$ axial reflections were measured on the film and corrected graphically. From these the cell parameters a and c and their e.s.d.'s for the α and β phases were claculated. The β angle was assumed to be that of Lukaszewicz and Nagler. These results are given in Table 4, Column 2. The e.s.d.'s are very high but the values of the parameters agree with those of Lukaszewicz and Nagler.

It was necessary to obtain better accuracy. A powder sample of α-$Cu_2P_2O_7$ was exposed for twenty-four hours in a Debye-Scherrer camera with CuKα radiation. The line separations corresponding to 4Θ were measured and corrected for film shrinkage in the normal manner. A program was prepared for use on the IBM 7040 computer (DESLID , Appendix 1) to aid in the identification of the Debye-Scherrer lines. Both the intensity of the lines, calculated from the parameters of the partially refined structure, and the 4Θ value, calculated from the data of Lukaszewicz and Nagler, for all possible reflections, could be compared with those observed. Thirty-nine lines were identified. A second program was prepared (DESLS, Appendix 1) which refined the reciprocal lattice parameters by non-linear least squares (Appendix 2). The real lattice parameters calculated by these programs are given in Table 4, column 3. The e.s.d.'s are based on the average discrepancy of 0.03% between observed and calculated d spacings.

The β parameters were found by measuring the difference between the values of Θ for the high angle axial α reflections and the corresponding β reflections. In this calculation, use was made of the following derived relationship between this $\Delta\Theta$ and the lattice parameters.

Let d^* be a reciprocal lattice spacing considered as a function of the observed Bragg angle Θ. Then, using a Taylor expansion

$$d^* (\Theta_H + \Delta\Theta_H) = d^*(\Theta)_H + \frac{\partial d^*(\Theta)_H}{\partial\Theta} \Delta\Theta_H + O (\Delta\Theta_H)^2 \qquad (1)$$

From the Bragg equation, $d^*_H = \frac{2 \sin \Theta_H}{\lambda}$

and

$$\Delta d^*_H = d^* (\Theta_H + \Delta\Theta_H) - d^*(\Theta)_H = \frac{2\Delta\Theta_H}{\lambda} \cos \Theta_H \qquad (2)$$

The e.s.d.'s are calculated from the relationship $\epsilon_\beta^2 = \epsilon_\alpha^2 + \epsilon_{\Delta p}^2$ where ϵ_β, ϵ_α and $\epsilon_{\Delta p}$ are respectively the e.s.d.'s of the β reciprocal lattice parameter, the α reciprocal lattice parameter and the change in the reciprocal lattice parameter. The percentage error in the real parameter is the same as that of the reciprocal lattice parameter provided that the β angle is expressed in terms of the cosine. It was observed that the maximum $\Delta\Theta_H$ occurred for H = (hoh). Δd^*_H for H = (808) was calculated from $\Delta\Theta_H$ to be $0.0068A^{-1}$. Δd^*_H was calculated to be $0.0061A^{-1}$ from the cell parameters determined above.

TABLE 4

Lattice Parameters of $Cu_2P_2O_7$

Compound	Axis	Lukaszewicz and Nagler	TiO Calibation	Debye-Scherrer lines
α-$Cu_2P_2O_7$	a	6.901 ± 0.005	6.89 ± 0.010	6.876 ± 0.002
	b	8.108 ± 0.005		8.113 ± 0.002
	c	9.176 ± 0.005	9.17 ± 0.015	9.162 ± 0.003
	β	109.65° ± 0.13°		109.54° ± 0.06°
β-$Cu_2P_2O_7$	a		6.88 ± 0.015	6.827 ± 0.004
	b			8.118 ± 0.005
	c		4.59 ± 0.02	4.576 ± 0.003
	β			108.85° ± 0.10°

CHAPTER 4: INTENSITY MEASUREMENT

(a) Logarithmic Optical Method

If an ordered series of n films are exposed to a constant source of X-rays successively for y min, yx min, --- yx^{n-1} min, then the relative intensities of a reflection on the successive films are given by $I_H(1) = I_H$, $I(2) = xI_H$, - - , $I_H(n) = x^{n-1} I_H$, provided that we assume the amount of darkening on the film remains proportional to the total number of incident photons. We can assign to a given reflection on the first film, a number z where $z = \ln_x I_H(1)$. Then on the j'th film, $j - 1 + z = \ln_x I(j)$. We can latter scale our measured intensities based upon an arbitrarily assigned intensity of x^z to a given reflection. Values of $\ln_x I_H$ for other H are estimated by comparing its intensity with the standard reflection and any number of previously estimated intensities, and by continual cross checking to maintain a consistent and reliable scaling.

In practice, the graduated exposures may be obtained by using the multiple film technique. Several films are loaded in the camera, interleafed with absorbing metallic films if necessary, and exposed in the normal manner. Now the j'th film will receive a diffracted beam of intensity $I_H(j) = \alpha^j I_H(1)$, where $I_H(1)$ is the beam incident on the first film and α is the fraction of the beam transmitted through the first film

$$\alpha = \exp(-\mu\rho x) \qquad (3)$$

where μ is the mass absorption co-efficient of the X-ray film, ρ the density of absorbing material and $\underline{x}$ is the distance travelled in the material. In the case of CuKα radiation the transmission of Ilford G film is near 36%, whereas for MoKα radiation, accurately rolled Cu foil must be inserted between the photographic plates.

The error in the measurement of $\ell n_x\ I_H$ is nearly constant in practice, increasing slightly at the high intensities. If we assume a constant error Δ, in $\ell n_x\ (I_H)$, then the error δ, in I_H, is given by

$$\pm \delta = I_H\ (e^{\pm\Delta} - 1) = \pm\ c\ I_H \qquad (4)$$

where c is a constant. The observed structure factor Fo_H is related to Io_H by $|Fo_H| = \sqrt{I_H/(L.P.)}$ where 1/L.P. represents the L.P. correction, the error , in Fo_H, is given by

$$\delta' = \frac{\delta}{2\sqrt{I_H}} = \frac{c}{2}\,|Fo_H|\ \left(\frac{1}{L.P.}\right)^{1/2} \qquad (5)$$

(b) The Diffractometer

Most of the {hk0} data reported in Tables 10 and 11 were recorded on a Supper single crystal diffractometer. The diffracted X-ray photons were detected by an Anton 202 Geiger-Muller tube containing a krypton-halogen mixture. The total dead-time, which includes the resolving time of the electronics, was measured to be 180 ± 30 μsec by the standard method as described by Evans (1955).

The number of pulses were counted with a Phillips PW 4032 Universal Scalar. The high voltage for the G.M. tube of 1300v was supplied by a Phillips PW 4029 Stabilized Supply Unit in conjunction with a PW 4024 High Voltage Supply. The pulses were amplifed by a PW 4072 Linear Amplifier and a PW 4082 discriminator was used to reduce the background. It was found that most of the background pulses originating in the electronics were an amplitude below 20v but that upon switching the motor on or off to oscillate the crystal, a supurious signal of 10 to 80 counts was recorded. This effect was eliminated by raising the discrimination voltage to 160v. The single pulses from the G.M. tube occurred at approximately 180v.

Because of the large number of photons in the diffracted beam and the relatively large dead-time of the system in a strong beam, the G.M. tube was easily overloaded to the point where coincidence losses caused an error of the order of 500%. Thus a system of filters was needed in order to reduce intensity of the diffracted beam such that coincidence losses were no greater than about 10%. The G. M. tube was supplied with a mechanism to allow easy insertion and interchange of filters but in order to avoid tedious adjustment of the G.M. tube position, a large aperature was required to allow all the photons in a diffracted beam to enter the chamber. Such a filter could not be used with this mechanism, so a new filter holder was designed as shown in Figure 3.

Sheets of absorbing material were placed in the hole in part A. These were held in place by gluing part B to part A. Three of these filters could be inserted in the holder (part C). The holder was bolted on the base of the G.M. tube in the same manner as the original filter holder. The filters were retained in position by the pin (D).

Zirconium filters were prepared for use with Molybdenum $K\alpha$ radiation. Eleven circular pieces of .007 in. Zr. sheet were cut. Filters were prepared by gluing together parts A and B with 1, 2, 4 and 4 of these Zr sheets enclosed. One could then choose any integral number of thicknesses of Zr sheet from 1 to 10, to be used as filter material.

Because there might be slight discrepencies in the thickness of the plates, the transmissivity of the filters had to be measured individually. The counter was set on a weak Bragg peak at low angle and the spindle drive was disengaged such that the X-rays were being continually diffracted, rather than rocking through the peak as in normal operation. One of the filters was used to decrease the counting rate further and to minimize dead-time correction. Also the percentage of the counts due to white radiation background was decreased because wave lengths other than $K\alpha$ have a different transmissivity through Zr. Each measurement was made with two filters, one to filter white background and one to be measured. Then each could be removed in turn to measure the count rate in its absence. Thus some readings were common to two filters.

During each measurement a number of counts were registered which were independent of the filter used and occurred even with the X-rays blocked off by closing the shutter on the generator beam port. These were due to stray radiation and cosmic rays from other apparatus in the vicinity. In general, stray radiation background counts were low (two counts per minute) and only increased when a beam port near the G.M. tube was open. Then the number of background counts were almost entirely due to cosmic rays, and depended on the tube position. The maximum count rate of 44 counts per minute occurred in the horizontal position ($2\theta = 0^{\circ}$). These count rates decreased slowly and uniformly to 39 counts per minute when the G.M. tube was vertical ($2\theta = 90^{\circ}$).

The count rate was determined over a period of 5 to 15 minutes with each crystal both "out" and "in" the beam. The time required to get accurate statistics for a given measurement depends on the count rate. The standard deviation in N counts is $\sqrt{N}$. Two or three readings were taken from each filter. The transmissivity was also measured using another reflection at a high value of 2θ. The number of counts for each reading was corrected for dead-time and normal background. The results are listed in Table 5. The values of the transmissivity for 4a and 4b show higher errors because of the bad statistics from the low intensity "in" beam. A stronger diffraction peak was not used for these filters because the results might be inconsistent with the other two filters. The values obtained at high angle represent a single reading with low e.s.d.'s and were averaged

with the low angle results. Also the predicted transmissivity is shown based on an average transmissivity per plate of 0.430. If the transmissivity per plate is α, the transmissivity of n plates is α^n. The transmissivity of white background by a filter depends on the distribution of wavelength in that background. This distribution varies with Θ and Ψ, the spindle angle (see Figure 4).* The distribution is altered by the filters through which the beam has previously passed. Thus the value of the background transmissivity reported is only an order of magnitude estimate.

Since the background varies by an upredictable amount in the region of a reflection, it should be measured on both sides of the reflection to minimize the error from background. Such a procedure would consume about 5 minutes in measuring the background for one reflection.

An attempt was made to determine a grid of the background as a function of Θ and Ψ at a sufficient number of points so that the background for any reflection might be determined by interpolation. For the case in hand this could be done in less than two hours.

In order to determine the number of counts to be subtracted from a reflection, one must know both the contribution of the background to the total count and the transmissivity of the combined filters used. Because of the dependence of transmissivity on wavelength, the total

---

* In Fig. 4 Ψ represents the relative spindle position

transmissivity is not necessarily equal to the product of the transmissivity of the individual filters, as would be the case for monochromatic radition. However, the error in the background intensity should be a second order effect, at least for reflections requiring more than one filter, and the discrepancy may be neglected. It is necessary, then, only to know the transmissivity of each filter used at all counting positions.

It was assumed that the transmissivity was not a function of Ψ and curves of transmissivity vs. Θ were obtained. However, in subsequent measurements it was found that the transmissivity depended on Ψ to such a large degree that effective transmissivity curves would have to be obtained for several values of Ψ. Therefore, it was decided that the most efficient way to measure background would be to make individual measurements in the vicinity of each reflection with the same filter that was used to measure that reflection, although the time consumed in obtaining these measurements would be large.

The intensity of a reflection is measured by "rocking" the crystal through a reflection position at a constant rate with the counter at a fixed angle. The values of Θ and Ψ were determined from a Weissenberg photograph of the same layer line with the same radiation. The counter was set at $2\Theta_H$ and the spindle was rotated to Ψ_H. The exact value of Ψ_H was found by listening for a marked increase in the count rate on the rate-meter speaker. The spindle was then centered on the peak and the

counter was rotated in both directions in turn until the count rate decreased. These positions were noted and the counter angle was set halfway between them. The spindle was rotated back from the maximum of the diffraction peak such that the rocking motion would carry the crystal completely through the diffraction peak and back again. The count rate was plotted on a chart recorder to insure that all the $K\alpha_1$ and $K\alpha_2$ reflections were counted. Very weak reflections could be found by observing the count rate on the recorder as the spindle was rocked through a wide angle.

The intensity of the reflection itself was first measured. Then to measure the background the spindle angle (Ψ) was changed such as to miss the peak on one side and then the other. Then the reflection whose intensity is equivalent by Friedel's Law was measured. In some cases either the background was sufficiently low, or the statistics were sufficiently poor that one or both of the two latter readings could be omitted.

It was found that dead-time losses could be kept to less than 10% if the total number of counts, with a normal rocking angle and rocking speed, were kept less than 6,000. Then by approximate dead-time corrections we could reduce the error to 2 or 3%. Since this is of the same order of magnitude as the statistical errors, further reduction is unwarranted.

(c) Corrections to Diffractometer Data

The data for the diffractometer must be corrected for several factors and normalized in some manner.

(i) Dead Time

This correction was performed by first fitting an approximate curve to the peak shape. The shape of a reflection as a function of Ψ is given by Zachariesen (1951) for a regular shaped crystal. However, the equation, in particular, for an irregularly shaped crystal, is very complex and impractical for calculation purposes. Furthermore, the shape of the crystals used in this work was not well know. Therefore, a Gaussian curve was fitted to the peak shape of a low angle reflection. The only discrepancies in the fitting occured at the ends of the curves and these were small. Thus, any reflection could be approximately constructed from two Gaussians, one for $K\alpha_1$ and for $K\alpha_2$ radiation and a constant background taken as the average of the two background reading.

Since the number of photons in the $K\alpha_1$ peak is known to be twice the number in the $K\alpha_2$ peak, the areas under the Gaussian curves, after subtracting the number of counts in the background, were taken as 2/3 and 1/3 respectively of the total number of counts in a reflection. The half-widths of the Gaussian were measured from the reflections recorded on the chart drive. It was found that these remained nearly

constant for all values of Θ and Ψ used. The separation between these Gaussians is a function of Θ. Differentiating the Bragg equations we obtain $\Delta\lambda = 2d\Delta\Theta \cos \Theta$ where then the separation of the $K\alpha$ peaks will correspond to a change in the spindle position ($\Delta\Psi$) since the spindle is rocked through the peak while Θ remains constant. For the geometry used, which is essentially that of a Weissenberg camera, the change in Θ is proportional to the change in Ψ in going from one reciprocal lattice point to another as a straight line can be drawn through those points and the origin. Then since $\frac{\Delta\lambda}{\lambda}$ is a constant, $\Delta\Psi = C \tan \Theta$ where C is some constant. A graph was drawn of $\Delta\Psi$ versus Θ. $\Delta\Psi$ was determined from reflections traced on the chart recorder. C was determined by fitting a curve of $C \tan \Theta$ to the experimental points.

The shape of the curve of an integrated reflection could now be predicted at any value Θ. The curve was broken into narrow strips and corrected for dead time. The strips were added to give the corrected number of counts for that reflection. This was repeated for the reflection whose intensity would be related by Freidel's Law. The background for that reflection was assumed to be in the same proportion to the total number of counts as for the first.

(ii) Background

The background was not corrected for dead-time because the low background count rate did not give rise to coincidence losses greater than 1%. The average background at each of the reflections labelled by H and -H was subtracted from the total number of counts previously corrected for dead time.

(iii) Rocking Angle

The time required to pass through one rocking motion was independent of the rocking angle. Thus the number of counts for a reflection was inversely proportional to the rocking angle since the reflection would be swept through faster if the angle was larger. Thus to "normalize" the intensity of a reflection, the number of counts were divided by the rocking angle.

(iv) Transmissivity of Filters

The number of counts for each reflection was divided by the product of the transmissivity of all filters used to measure it, in order that a normalized intensity might be obtained, corresponding to no filters or dead-time.

(v) Incident Beam Intensity

The intensity of the beam incident on the crystal was altered during the course of the measurement. The change in the incident beam was obtained by measuring the intensities of several strong reflections and finding the ratio of the new readings to the old. The intensities of reflections measured after this point had to be multiplied by this ratio.

A program was prepared for use on the 7040 computer to perform the above operations (DIC, Appendix 1). The program also calculated an error based on counting statistics and other experimental errors.

TABLE 5

Transmissivity of Zirconium Filters

Filter	No. thicknesses of 0.007' foil	Low Angle Reflection	High Angle Reflection	Calculated Assuming 0.007' / Foil	Average	White Background
1	1	.431	.433	.430	.432 ± .003	.182
2	2	.184	.182	.185	.183 ± .003	.081
4a	4	.0342	.0349	.0342	.0345 ± .0010	.021
4b	4	.0346	.0359	.0342	.0352 ± .0010	.022

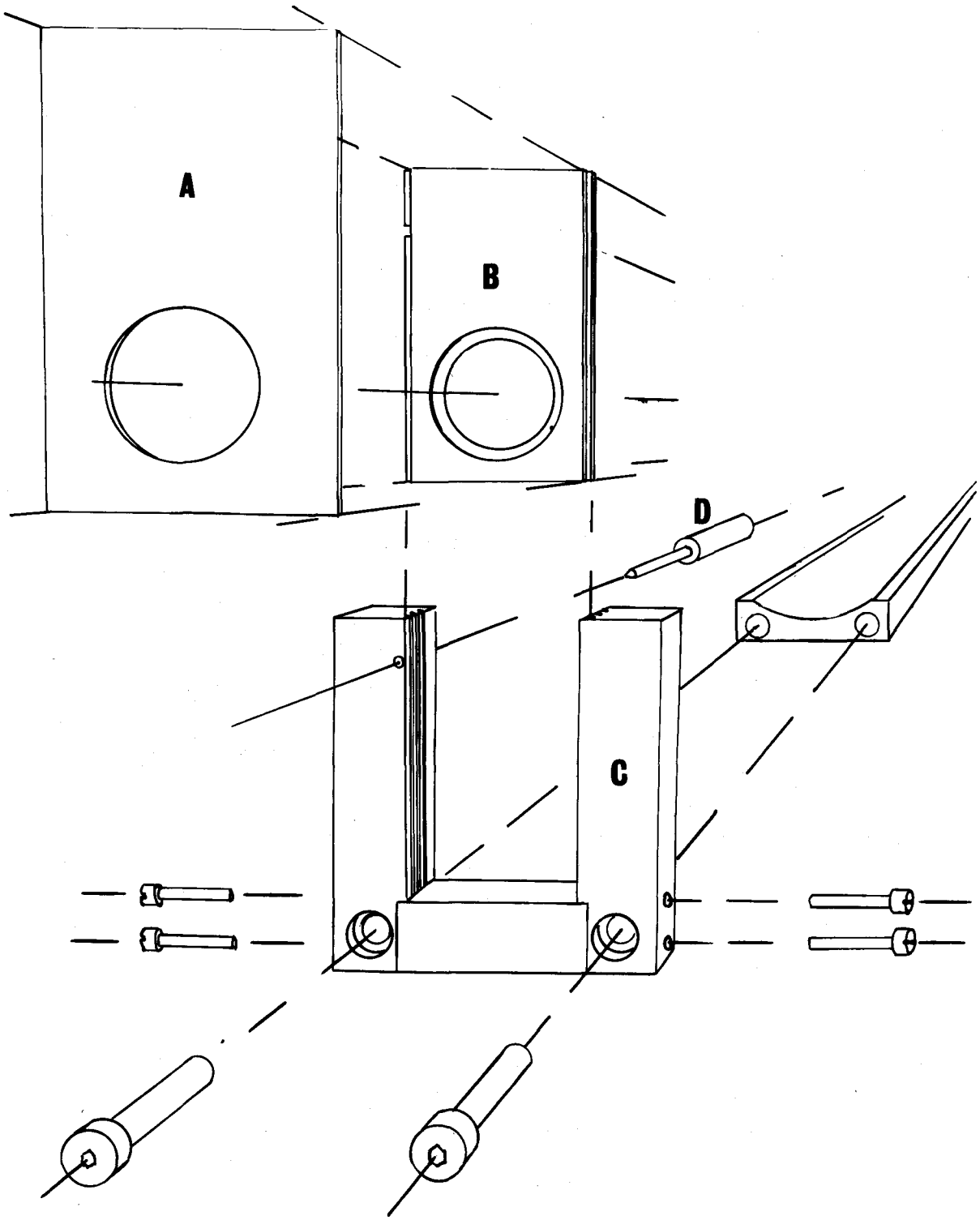

Fig.3

Filter Holder for Diffractometer

Fig.4

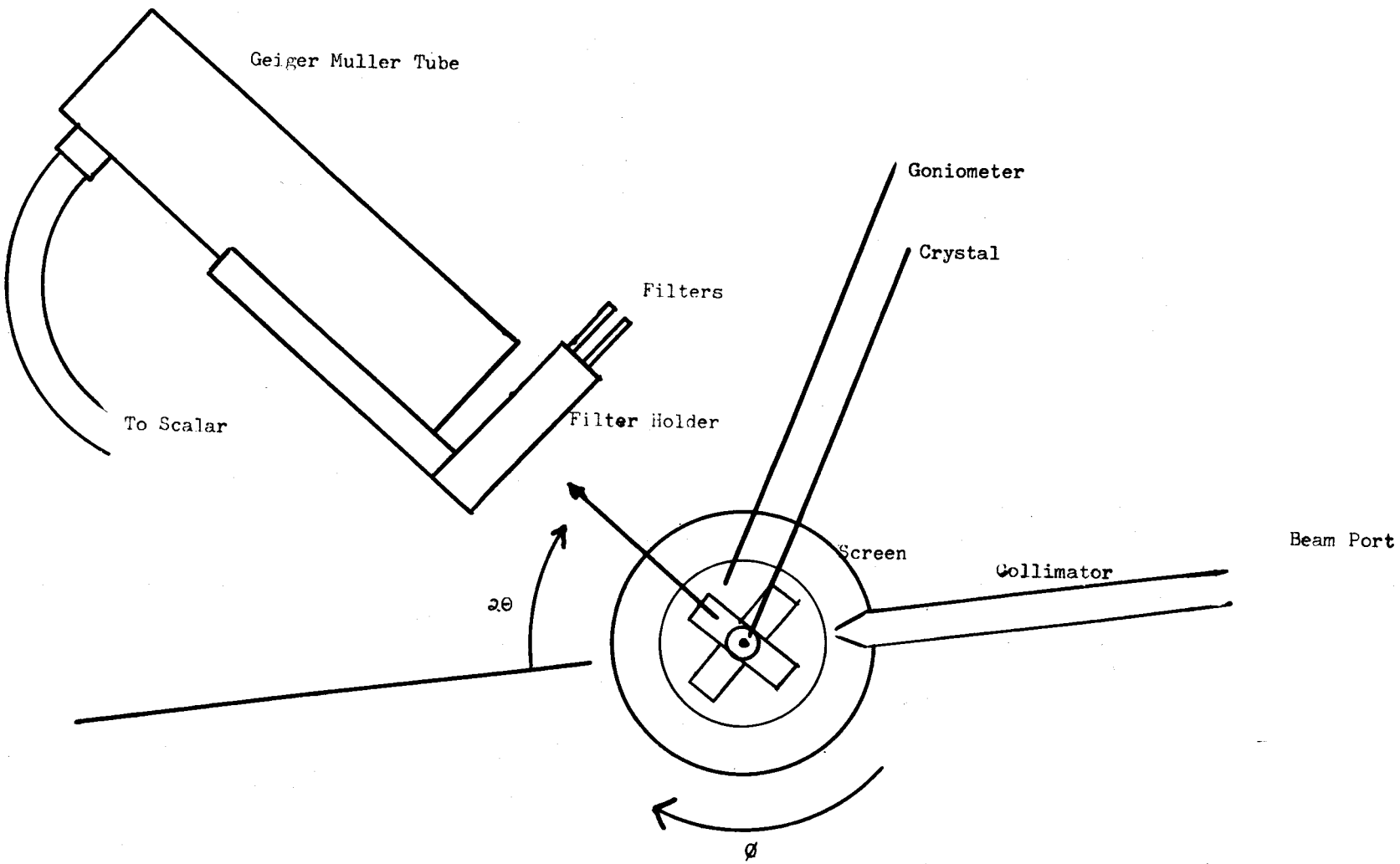

Geometry of Diffractometer

CHAPTER 5: REFINEMENT

(a) Data

Multiple film Weissenberg photographs using CuKα radiation were taken with the crystal aligned about the b axis. The room temperature and 200°C exposures were superimposed on the same film with the camera displaced between exposures. In addition, Weissenberg photographs were taken containing reflections of the type $\{hk\ell\}$ with $0 \leqslant \ell \leqslant 4$ at room temperature using CuKα radiation. Since the odd layer lines corresponding to the α phase were absent in the β form, only the comparable $\{hk0\}$, $\{hk1\}$ and $\{hk2\}$ reflections could be photographed. These were taken at 100°C. At present only data of the type $\{hk1\}$ for both phases and $\{hk2\}$ for the α phase have been measured.

The diffractometer was used to determine the intensities, of reflections of the $\{hk0\}$ zone for both phases. These data were recorded at 100°C by heating the crystals with a hair dryer. It is to be noted that the same crystal was used in both photographic and counter measurements. The temperature was monitored with each reading and varied over less than 8°C. MoKα radiation was used because many strong reflections occurred in the region beyond the CuKα sphere. $\{0k\ell\}$ photographs of the α phase of the same crystal were taken with the precession camera, using MoKα radiation.

As a check on the effect of anomalous absorption of CuKα radiation in $Cu_2P_2O_7$, the intensities of the $\{h0\ell\}$ reflections from the α phase were remeasured from a photograph taken with MoKα radiation on the precession camera. A new crystal was chosen because there was some danger that the stycast, used to cement the crystals previously employed to obtain the $\{h0\ell\}$ photographs, might have covered the crystal in such a manner as to effect the intensity distribution.

A summary of the data used in this study is found in Table 6 together with the number of independent observations in each layer line of data. All films were measured by the logarithmic technique.

(b) High Temperature Structure

Because other members of the "transition metal ion" pyrophosphate series had been shown to belong to the space group C 2/m, this space group was used throughout the refinement of the structure. The intensities of the 38 $\{ho\ell\}$ reflections were corrected for the effect of the Lorentz-polarization factor and converted to relative structure factors by taking the square root of the resultant magnitude. The atomic parameters of β-$Zn_2P_2O_7$ were used as trial values to calculate the structure factors for β-$Cu_2P_2O_7$. The structure factors are given by

$$Fc_H = \sum_j f_{j_H} \exp(2\pi i \vec{H}_i \cdot \vec{r}) \qquad (6)$$

where H is the set of Miller indices $\{hk\ell\}$, and f_j is the scattering

TABLE 6

Measured Data

Layer Line		Rad.	Method of Recording	Temp.	No. of Nodes
β-$Cu_2P_2O_7$	$\{h0\ell\}$	CuK_α	Multiple film Weissenberg	200°C.	38
	$\{hk0\}$	MoK_α	Diffractometer	100°C	170
	$\{hk1\}$	CuK_α	Multiple film Weissenberg	100°C	67
α-$Cu_2P_2O_7$	$\{h0\ell\}$	CuK_α	Multiple film Weissenberg	Approx. 20°	38
	$\{h0\ell\}$	MoK_α	Precession	" "	40
	$\{hk0\}$	MoK_α	Diffractometer	" "	170
	$\{hk1\}$	CuK_α	Multiple film Weissenberg	" "	62
	$\{hk2\}$	CuK_α	Multiple film Weissenberg	" "	67
	$\{0k\ell\}$	MoK_α	Precession	" "	55

factor of the j'th atom in the unit cell. f_j must be evaluated at the value of sin θ/λ corresponding to H . $\vec{r}$ is the set of atomic co-ordinates of the j'th atom expressed in terms of fractions of the unit cell edges. The sum is over the atoms in one unit cell. The terms for symmetry related atoms may be combined to give trigonometric functions and thus lower the number of terms in the summation to those atoms in an asymmetric zone. This calculation was performed with the Bendix G-15 computer.

In order to account for thermal motion of the atoms in the crystal, it is necessary to multiply F_{c_H} by exp $(-\vec{H}.\underline{\underline{B}}.\vec{H})$ where $\underline{\underline{B}}$ is a second order tensor. As a first approximation, one may assume the thermal motion to be isotropic, and then $\underline{\underline{B}}$ may be represented by a scalar, B. In the process of finding B, it is necessary to find a scale constant k, since B and k are highly correlated. That is,

$$k \left| F_{o_H} \right| = \left| F_{c_H} \right| \exp\left(-B \sin^2 \theta/\lambda^2\right) \tag{7}$$

or

$$-\ln\left(F_{o_H}/F_{c_H}\right) = \ln k + B \sin^2 \theta/\lambda^2 \tag{8}$$

Now, the two sides of the latter equation may be fitted by linear least squares. This procedure was applied to the $\{ho\ell\}$ data.

The commonly used measure of discrepancy between the observed and calculated structure factors is the R factor (reliability factor) defined as

$$R = \frac{\sum_H \left| |F_{o_H}| - |F_{c_H}| \right|}{\sum_H |F_{o_H}|} \qquad (9)$$

where F_{o_H} and F_{c_H} are the observed and calculated structure factors, For all reliability factors given here, both sums are only over observed reflections, excluding those not entered into least squares refinement as will be discussed later.

The relatively low R factor of .302, obtained at this stage, suggested that the proposed structure might be approximately correct. Therefore, an electron density distribution was prepared using the phases of the calculated structure factors determined from these trial co-ordinates.

The density of electrons at a point in the unit cell defined by the fractional co-ordinate $\vec{r}$ is give by

$$\rho(r) = \frac{1}{v} \sum_H F_{o_H} \exp(-2\pi i \vec{H}.\vec{r}) \qquad (10)$$

where v is the volume of the unit cell. The sum is over all reciprocal lattice points H, but in practice, H is limited by the fact that $|\sin \theta| \leq 1$. However, the structure factors are small at high values of θ because the electrons are distributed over a finite volume in real space. Thus a good approximation for ρ usually may be determined from a finite sum of terms out to the Ewald sphere. Now if we calculate the projection of ρ onto one face of the unit cell, say the $\underline{y} = 0$ face,

we may define σ as

$$\sigma\ (x,\ z) = \int_0^1 \rho\,(x,\ y,\ z)\ \ b\ dy \tag{11}$$

Then

$$\sigma(x,\ z) = \frac{1}{S} \sum_H F_{o_H} \exp\left\{-2\pi i\ (hx + \ell z)\right\}$$

$$\int_0^1 \exp\ (-2\pi iky)\ dy \tag{12}$$

where S is the cross-sectional area of the unit cell in the $\underline{y} = 0$ plane. But the integral is zero unless $\underline{k} = 0$, and therefore, only members of the vector set H with $\underline{k} = 0$ contribute.

σ (x, z) was calculated using Beevers-Lipson strips. From the peaks of electron density, improved atomic co-ordinates were determined. If one substitutes $(Fo_H - Fc_H)$ in place of Fo_H in the electron density projection formula, the Fourier sum becomes $\sigma_o - \sigma_c$ where σ_o and σ_c are the observed and calculated electron distribution projections respectively.

The signs assigned to Fo_H are usually assumed to be the same as those calculated for Fc_H. Corrections to the atomic parameter may be determined from the slope of the difference Fourier synthesis (Lipson and Cochran (1953)). The new $\underline{x}$ and $\underline{z}$ co-ordinates obtained from the

electron density projection were used to calculate new structure factors using the Bendix G-15 computer with the program SF-10 (Appendix 1). These were used to calculate a new difference synthesis. From this map, new co-ordinates were obtained. By this procedure the R factor was lowered to 0.26. A program to calculate structure factors was later prepared for use on the IBM 1620, Model 1 Computer, allowing for individual temperature factors for each atom (SF-20, Appendix 1). The R factor was promptly lowered to 0.20, since the central oxygen and the Cu^{++} ion had large temperature factors.

The 110 observed and 60 unobserved $\{hk0\}$ reflections were corrected for counting errors and Lorentz-polarization effects (see Diffractometer Corrections) and converted to structure factors with standard deviations. The calculations were done using the 7040 program DP-IV (Appendix 1). The 7040 program SAC (Appendix 1) was used for structure factor calculations in this zone. This program also calculated an isotropic overall temperature factor and scale constant and applied these to the data. The $\underline{y}$ co-ordinates for β-$Zn_2P_2O_7$ were used with the refined $\underline{x}$ co-ordinates of β-$Cu_2P_2O_7$ to calculate the structure factors for the $\{hk0\}$ zone. A reliability value of 0.51 was found. An electron density distribution was calculated from these co-ordinates. From this map new co-ordinates were obtained which gave an R factor of 0.32. This procedure was repeated and gave an R factor of 0.21.

The observed structure factors and their e.s.d.'s were calculated from the intensities and e.s.d.'s of the 67 measured hkl reflections. Also e.s.d.'s were calculated for hoℓ reflections. All e.s.d's were taken as some fraction of $|Fo_H|$, depending on the accuracy with which $|Fo_H|$ was measured. All the observations were entered into a cystallographic least squares calculation using the 7040 program MACLS (Appendix 1). The overall R factor was refined down to 0.165 using individual isotropic temperature factors in addition to atomic co-ordinates as variables.

In an effort to determine if the effect of the anomolous absorption of CuKα radiation by Cu^{++} were significant, the Cu^{++} scattering curve was altered to allow for the anomolous scattering and the data taken with CuKα radiation were refined using both corrected and uncorrected scattering curves for Cu^{++}. A slightly better R factor was obtained using the uncorrected scattering curve, so it was assumed that the errors from anomolous scattering were not large enough to cause any significant errors in the results. Furthermore, there was no easy way of allowing for anomolous scattering in the computer programs available, since only one scattering curve was allowed per species of atom and MoKα radiation had been used to obtain the (001) zone.

For some of the reflections, very large discrepancies between Fo_H and Fc_H were found. Also some extraneous spots appeared on all the films. This suggested that some reflections with large discrepancies might be affected by secondary extinctions. Also, very strong reflections

could not be measured accurately in some cases because the scale of intensities provided no reflections for comparison. These reflections with large discrepancies were given zero weight in the least square requirement.

The atomic co-ordinates were further refined using anisotropic temperature factors for each atom. After several cycles of refinement an R factor of 0.135 was obtained. The agreement in some of the reflections that had been given zero weight had now improved sufficiently so that they could be added into the refinement. The structure was further refined, but no significant changes occurred in the atomic co-ordinates and the R factor did not decrease appreciably. The final co-ordinates and temperature factor components are listed in Table 7. The observed and calculated structure factors are listed in Table 10. The pertinent interatomic distances and angles were calculated using the 7040 program BAT (Appendix 1). These are listed in Table 12.

TABLE 7

Fractional Atomic Coordinates and Anisotropic Temperature Factor

Components in β-$Cu_2P_2O_7$ (e.s.d.'s in parenthesis)

Atom	Point Symmetry	x/a	y/b	z/c	β_{11}	β_{22}	β_{33}	β_{12}	β_{13}	β_{23}
Cu	2	0	0.3126 (.0003)	1/2	0.0102	0.0028	0.0441	0	-0.0029	0
P	m	0.1998 (0.0008)	0	-0.0842 (0.0040)	0.0051	0.0035	-0.0401	0	-0.0037	0
O_1	$\bar{1}$	0	0	0	0.0004	0.0278	-0.0245	0	-0.0332	0
O_3	1	0.1998 (0.0021)	0.1493 (0.0011)	-0.2666 (0.0142)	0.0123	0.0035	0.0524	0.0030	-0.0098	-0.0011

(c) The Low Temperature Structure

The space group of α-$Cu_2P_2O_7$ is either C 2/c or C c as mentioned in the introduction. In both space groups the Cu^{++} ions are allowed to move away from the two fold axis passing through them in the β phase. Since they are heavy scatterers, this displacement will probably account for a large portion of the change in the structure factors from their values in the β phase. These should presumably be moved off the two fold axis in the direction of the major axis of the high temperature vibrational ellipsoid to obtain trial parameters for the α phase. This will also avoid zero diagonal elements in the normal equations of the least squares refinement. All atomic displacements must be consistent with the space group C 2/c or C c. However, there is an arbitrary choice as to which Cu^{++} atom goes in the positive direction and which goes in the negative direction. Each choice may give a least squares minimum, but only one choice bears the proper relation to the displacement of the other atoms in the unit cell. In particular the Cu^{++} displacement must be consistent with the bending of the P-O-P angle. One of these alternatives was chosen and the central oxygen atom was moved up the b axis.

The 38 $\{ho\ell\}$ structure factors observed with CuKα radiation were calculated from the measured intensities. R factors were obtained for this data using the above mentioned positions in both C 2/c and C c space groups. The 1620 program SF-30 (Appendix 1) was used for these calculations. R, using the parameters obeying the symmetry of the space group C 2/c was 0.36, and using the parameters for the space group C c, 0.29. C c was then chosen as the trial space group. An attempt was made to refine

the x and z co-ordinates using both electron density distributions and difference synthesis. However, the best R factor that could be obtained by these methods using this limited amount of data was 0.27.

The intensities of the 170 reflections in the (001) zone were converted to structure factors. The x co-ordinates from the α-$Cu_2P_2O_7$ σ(x, z) projection and the y co-ordinates from the β-$Cu_2P_2O_7$ σ(x, y) projection were used to calculate structure factors which gave an R factor of 0.36. This was lowered to 0.27 by using the atomic displacements obtained from an electron density distribution calculation. The improved x co-ordinates were substituted into a structure factor calculation with the {hol} reflections. The R factor for this data was lowered to 0.24. However, no further improvements in the agreement could be made on either projection by difference synthesis analysis. These data were then entered into a least squares analysis using isotropic temperature factors. Several groupings of the co-ordinates were varied, but for each combination the analysis diverged. About thirty reflections with very poor agreement between Fo_H and Fc_H were given zero weight in the least squares analysis. The least squares analysis converged if only the Cu^{++} and P atomic parameters were allowed to vary. Varying all the parameters with an isotropic temperature factor and with the proper weighting lead to an R factor of 0.22. Anisotropic temperature factors were used but the R factor could not be lowered below 0.18 by further least squares analysis.

Since the Fo_H cannot be accurately determined it is necessary for the ratio of the number of observations to the number of variables be considerably greater than 1. This ratio is referred to as the over-determinancy of the refinement. More data were required to refine properly the 97 variables present in the C c space group. The 55 $\{0k\ell\}$ structure factors were calculated from the measured intensities taken from precession films. Also the 62 $\{hk1\}$ and 67 $\{hk2\}$ reflections from Weissenberg photographs were measured and processed into Fo_H. These data were added to the $\{ho\ell\}$ and $\{hko\}$ data and further least squares refinements were carried out until an R factor of 0.16 was obtained.

The greatest discrepancies occurred among the $\{hkl\}$ reflections. Since they were all absent in the high temperature form, these were most sensitive to the departures from C 2/m symmetry. This indicated that the previous choice of the Cu^{++} displacement was in the wrong direction in relation to the bending of the P-O-P angle. The alternative choice was used and, after two more cycles of refinement, the R factor dropped to 0.13 and the agreement between the $\{hkl\}$ Fo_H and Fc_H was as good as for the other layer lines.

The $\{ho\ell\}$ reflections still contained a large number of reflections with poor agreement. Both the measurement of the intensities and the Lorentz-polarization corrections for these refections were throughly re-checked, but no inconsistencies were found. However, it was possible

that there were serious absorption losses from the high temperature glue which nearly covered the crystal used to measure these reflections. The 40{h0ℓ} precession reflections were corrected by the Lorentz-polarization factor and substituted into the refinement. These reflections were photographed with MoKα radiation and thus their intensities would serve as a check on the anomolous absorption effects of the CuKα radiation. Only small random differences were noted between the Fo_H obtained with this radiation and those obtained previously. Thus no significant improvements occurred in the least squares refinement, using the new data.

The refinement now appeared completely convergent. However, the bonds calculated with these co-ordinates (Table 8) were not realistic chemically. The P-O(P) bonds were 1.80 and 1.38A and the other P-O bonds were widely varying. The lengths of P-O bonds of order 1 and 2 are 1.71A and 1.38 A respectively. The order of these bonds should be between 1 and 2 and the errors in their lengths are about .05A. The Cu^{++} -O bonds lengths were also of unusual magnitude. Trial atomic positions were obtained by averaging these bond lengths such that the symmetry of the crystal was C 2/c. Also the origin was displaced a distance c/4 in order to lie on the center of symmetry. The Cu^{++} ions were related by a center of symmetry and the central oxygen atom in the b direction. Three cycles of refinement were carried out in the space group C 2/c and the R factor was lowered to 0.131. The bond lengths

TABLE 8

α-$Cu_2P_2O_7$ Bond Lengths in Space Group C-c

Bond	Bond Length (A)	Bond	Bond Length (A)
P_1-O_1	1.383	Cu_1-O_{21}	2.003
P_2-O_1	1.802	Cu_1-O_{22}	1.811
P_1-O_{21}	1.504	Cu_1-O_{31}	2.318
P_2-O_{22}	1.838	Cu_1-O_{32}	2.947
P_1-O_{31}	1.578	Cu_1-O_{33}	1.939
P_1-O_{34}	1.565	Cu_1-O_{34}	1.814
P_2-O_{32}	1.421	Cu_2-O_{21}	2.045
P_2-O_{33}	1.490	Cu_2-O_{22}	1.826
		Cu_2-O_{31}	1.929
		Cu_2-O_{32}	1.997
		Cu_2-O_{33}	2.291
		Cu_2-O_{34}	3.053

calculated from these co-ordinates, except possibly for one Cu^{++}-O bond, were more realistic. The atomic parameters and molecular geometry are given in Tables 9 and 13 respectively.

TABLE 9

Fractional Atomic Coordinates and Anisotropic Temperature Factor Components of

α-$Cu_2P_2O_7$ in Space Group C 2/c (e.s.d.'s in parenthesis)

Atom	Point Set	x/a	y/b	z/c	β_{11}	β_{22}	β_{33}	β_{12}	β_{13}	β_{23}
Cu	1	0.0199 (0.0011)	-0.3129 (0.0003)	0.4923 (0.0005)	0.0032	0.0024	0.0016	0.0003	-0.0007	-0.0001
P	1	0.1983 (0.0010)	0.0090 (.0007)	0.2043 (0.0017)	0.0029	0.0024	0.0009	-0.0001	0.0003	0.0000
O_1	2	0	0.0490 (0.0037)	1/4	0.0029	0.0123	0.0026	0	0.0018	0
O_2	1	0.3790 (0.0030)	-0.0025 (0.0015)	0.3642 (0.0039)	0.0063	0.0061	0.0006	0.0004	0.0047	0.0029
O_{31}	1	0.2222 (0.0026)	0.1594 (0.0012)	0.1141 (0.0030)	0.0009	0.0025	-0.0008	-0.0008	-0.0015	0.0009
O_{32}	1	0.1739 (0.0029)	-0.1551 (0.0018)	0.1214 (0.0028)	0.0038	0.0025	-0.0008	0.0012	-0.0007	0.0001

Table 10 Observed and Calculated Structure Factors for β-$Cu_2P_2O_7$

H	K	L	F(O)	F(C)	H	K	L	F(O)	F(C)	H	K	L	F(O)	F(C)	H	K	L	F(O)	F(C)
0	0	1	49.4	-40.6	5	5	1	61.4	61.8	2	18	0	7.7	-9.0	12	6	0	1.2	-1.7
0	0	2	55.4	47.0	3	5	1	16.7	14.6	2	20	0	1.2	-3.6	12	8	0	7.1	-9.5
0	0	3	63.5	-41.3	1	5	1	60.4	75.1	3	1	0	45.7	-55.1	13	1	0	2.9	-3.6
0	0	4	52.7	52.1	-5	1	1	46.1	45.5	3	3	0	64.9	77.9	14	0	0	2.9	7.4
0	0	5	49.6	-48.9	-3	5	1	48.2	52.7	3	5	0	61.0	-63.2	4	20	0	<1.8	-0.1
2	0	1	38.3	-39.7	-5	5	1	57.7	51.9	3	7	0	4.4	-5.8	3	17	0	<2.3	-2.9
2	0	2	113.8	94.5	-7	5	1	7.7	7.0	3	9	0	9.5	7.6	5	15	0	<2.4	2.5
2	0	3	65.2	-50.2	4	6	1	50.8	-42.3	3	11	0	31.8	-25.0	6	14	0	<2.4	-4.6
2	0	4	62.0	62.1	2	6	1	27.1	-25.7	3	13	0	11.5	8.5	7	9	0	<2.1	0.0
-2	0	2	74.2	68.3	-6	2	1	39.1	38.3	3	15	0	10.0	-9.1	7	13	0	<2.4	0.8
-2	0	3	51.6	-30.2	-4	6	1	<14.3	-2.1	3	19	0	3.3	6.1	7	15	0	<2.3	-6.7
-2	0	4	36.3	37.5	-6	6	1	31.4	-22.8	3	21	0	5.3	-7.4	7	17	0	<2.1	-4.0
-2	0	5	15.3	-15.0	5	7	1	11.2	8.3	4	2	0	44.3	-44.4	8	6	0	<2.0	4.2
4	0	0	70.3	78.1	3	7	1	48.8	-48.5	4	4	0	2.0	-1.8	8	12	0	<2.4	-2.2
4	0	1	79.1	-82.8	1	7	1	11.9	8.0	4	6	0	34.8	36.4	8	16	0	<2.2	6.4
4	0	2	46.2	41.0	*-7	1	1	30.8	-8.0	4	8	0	37.5	-34.0	8	18	0	<1.8	-2.7
4	0	3	48.5	-49.4	-3	7	1	14.8	-9.6	4	10	0	17.6	15.1	9	1	0	<2.0	-1.1
*-4	0	2	68.3	104.6	-5	7	1	<14.5	2.0	4	12	0	1.4	1.6	9	9	0	<2.3	3.2
-4	0	3	14.6	11.4	4	8	1	26.3	23.8	4	14	0	7.4	-11.1	9	13	0	<2.4	8.3
-4	0	4	50.9	57.7	2	8	1	37.8	43.5	4	16	0	7.1	8.7	9	15	0	<2.2	-3.7
-4	0	5	17.5	18.1	-8	2	1	14.0	13.3	4	18	0	5.6	-6.3	9	17	0	<1.8	-2.2
6	0	1	16.7	-13.0	-4	8	1	50.6	49.2	5	1	0	28.3	30.3	10	8	0	<2.3	-0.8
6	0	2	58.4	50.3	3	9	1	32.5	-29.3	5	3	0	59.4	64.1	10	12	0	<2.4	4.9
-6	0	1	47.9	-40.6	1	9	1	19.1	-10.9	5	5	0	7.8	-8.1	10	14	0	<2.2	1.0
-6	0	2	24.0	28.5	-3	9	1	24.7	-18.8	5	7	0	42.7	44.7	10	16	0	<1.9	5.1
-6	0	3	42.1	-33.5	* 0	2	1	69.0	119.6	5	9	0	22.9	22.6	11	5	0	<2.3	-3.8
-6	0	4	11.2	10.1	0	4	1	42.2	40.4	5	11	0	4.6	-9.2	11	7	0	<2.4	7.4
-6	0	5	23.8	24.5	0	6	1	18.0	-16.0	5	13	0	34.2	28.0	11	9	0	<2.4	5.8
8	0	0	12.2	12.1	0	8	1	58.1	63.2	5	17	0	7.4	-1.8	11	11	0	<2.3	-4.4
-8	0	1	23.2	-18.0	-1	9	1	9.5	-6.8	5	19	0	8.8	10.7	11	13	0	<2.2	5.9
-8	0	2	29.0	32.3	-2	8	1	11.9	9.7	6	0	0	49.3	56.5	11	15	0	<1.8	0.9
-8	0	3	<14.7	17.9	-2	10	1	41.2	-37.0	6	2	0	17.5	-16.9	12	10	0	<2.3	0.9
*-2	0	1	75.2	-168.1	-4	2	1	66.0	67.9	6	4	0	3.5	5.1	12	12	0	<2.1	-3.8
-4	0	1	6.8	-7.9	0	2	0	7.3	3.3	6	6	0	29.0	28.3	12	14	0	<1.8	-5.1
7	1	1	19.5	13.8	0	4	0	32.3	30.1	6	8	0	20.5	-16.1	12	16	0	<1.3	1.8
5	1	1	48.2	51.1	0	10	0	37.6	35.1	6	10	0	17.6	14.7	13	3	0	<2.4	4.2
3	1	1	23.2	-21.5	0	12	0	20.9	18.0	6	12	0	3.6	0.9	13	5	0	<2.4	-5.6
* 1	1	1	49.0	87.1	0	14	0	3.7	3.1	7	1	0	32.9	-30.9	13	7	0	<2.3	-1.3
-1	1	1	27.0	30.1	0	16	0	22.8	18.4	7	3	0	16.9	18.3	13	9	0	<2.2	-0.1
-1	3	1	26.0	-25.8	0	18	0	2.4	-3.1	7	5	0	41.6	-37.9	13	11	0	<2.0	-3.5
-1	5	1	56.5	68.2	0	20	0	4.2	6.0	7	7	0	10.7	-9.1	13	13	0	<1.7	0.7
-1	7	1	35.2	-31.5	1	1	0	18.8	-18.3	7	11	0	24.7	-19.3	14	2	0	<2.3	0.4
6	2	1	41.3	33.2	1	3	0	62.8	75.6	8	2	0	22.7	-20.3	14	4	0	<2.3	2.4
4	2	1	39.7	43.0	* 1	5	0	88.8	-63.4	8	4	0	2.4	-1.3	14	6	0	<2.2	4.4
2	2	1	47.0	62.7	1	7	0	27.9	27.8	8	8	0	23.9	-22.3	14	8	0	<2.1	-2.1
-2	2	1	14.6	13.1	1	9	0	13.8	14.8	8	10	0	9.7	8.6	14	10	0	<1.9	2.2
-2	4	1	33.1	-29.9	1	11	0	31.0	-27.8	8	14	0	10.3	-10.1	14	12	0	<1.6	1.1
-2	6	1	62.2	-78.9	1	13	0	26.7	21.3	9	3	0	15.8	17.5	15	1	0	<2.2	4.3
7	3	1	32.8	-30.9	1	15	0	9.1	-5.6	9	5	0	13.2	-9.8	15	3	0	<2.2	6.1
5	3	1	<14.2	-6.9	1	17	0	4.4	-6.3	9	7	0	4.0	7.3	15	5	0	<2.1	1.3
3	3	1	64.8	-84.1	1	19	0	7.1	8.1	9	11	0	5.5	-7.3	15	7	0	<1.9	4.0
1	3	1	60.0	-86.7	1	21	0	6.0	-6.0	10	0	0	31.9	30.6	15	9	0	<1.7	2.4
-3	1	1	44.3	53.3	2	0	0	29.0	30.0	10	2	0	5.9	3.3	16	6	0	<1.7	2.9
-3	3	1	60.6	-73.1	2	2	0	57.9	-73.0	10	4	0	11.0	8.7	16	4	0	<1.8	2.2
-5	3	1	19.5	-17.0	2	4	0	1.6	-1.0	10	6	0	22.1	19.6	16	0	0	<1.9	5.2
-7	3	1	56.5	-38.5	2	6	0	7.6	8.6	10	10	0	5.9	8.4	17	1	0	<1.6	-0.3
6	4	1	<14.2	2.6	2	8	0	59.8	-61.2	11	1	0	2.1	3.7	18	0	0	<1.0	1.4
4	4	1	9.4	10.5	2	10	0	21.3	18.2	11	3	0	16.4	13.7	17	5	0	<1.5	-1.7
2	4	1	12.5	-7.7	2	12	0	14.7	-10.7	12	0	0	2.4	1.3	17	3	0	<1.6	1.2
-4	4	1	13.8	11.3	2	14	0	25.1	-22.0	12	2	0	7.1	-8.4					
-6	4	1	19.7	13.1	2	16	0	18.4	12.3	12	4	0	1.4	-3.4					

* Unreliable

Table 11 Observed and Calculated Structure Factors for α-$Cu_2P_2O_7$

H	K	L	F(O)	F(C)	H	K	L	F(O)	F(C)	H	K	L	F(O)	F(C)	H	K	L	F(O)	F(C)
0	4	0	29.8	29.8	12	6	0	3.6	-5.9	-5	7	1	16.7	16.2	-3	5	2	45.0	-51.6
0	6	0	98.5	104.5	12	8	0	4.9	-6.5	2	8	1	11.9	8.7	-5	5	2	55.1	-50.3
0	8	0	23.0	-23.1	6	0	0	41.7	54.4	0	8	1	10.1	-10.0	-7	5	2	11.4	6.3
0	12	0	23.7	20.6	4	0	0	73.0	74.1	-2	8	1	9.0	7.2	4	6	2	48.6	50.2
0	14	0	2.9	-4.2	2	0	0	24.6	31.3	-4	8	1	12.4	-10.1	-6	2	2	35.5	-34.7
0	16	0	13.3	14.7	-4	0	2	5.8	8.4	-8	2	1	32.2	-32.8	2	6	2	24.6	28.8
0	18	0	2.5	-2.4	*-2	0	2	113.0	175.6	3	9	1	20.1	18.5	-4	6	2	< 8.4	2.6
0	20	0	1.2	3.3	2	0	2	46.1	42.5	1	9	1	< 4.4	-2.6	-6	6	2	31.5	24.7
1	1	0	21.3	-19.6	4	0	2	87.8	86.5	-1	9	1	9.3	-7.1	5	7	2	11.6	-3.0
1	3	0	69.2	72.6	6	0	2	11.1	12.4	-3	9	1	14.5	-11.1	3	7	2	49.1	47.0
1	5	0	65.2	-63.4	8	0	2	52.0	38.2	0	10	1	6.5	-6.3	1	7	2	11.1	-4.8
1	7	0	28.3	24.8	-8	0	4	18.7	15.2	-2	10	1	15.0	13.9	-7	1	2	30.2	19.0
1	9	0	15.9	13.0	-6	0	4	22.4	17.6	0	0	6	64.4	62.1	-3	7	2	15.3	12.1
1	11	0	33.7	-27.4	-4	0	4	76.4	99.7	0	0	8	59.9	63.5	-5	7	2	< 8.1	-2.2
1	13	0	28.8	23.8	-2	0	4	63.6	78.4	0	2	0	6.0	-4.4	4	8	2	26.5	-28.2
1	15	0	5.1	-6.7	2	0	4	84.2	112.3	0	2	2	88.8	-118.6	2	8	2	37.1	-39.5
1	17	0	5.9	-6.0	4	0	4	59.2	46.4	0	2	3	2.4	-1.9	-8	2	2	< 6.7	-5.4
1	19	0	7.7	11.4	6	0	4	72.6	52.3	0	2	4	50.3	-37.7	-4	8	2	50.9	-42.3
1	21	0	4.5	-7.4	-8	0	6	< 12.1	-2.8	0	2	5	20.9	-20.5	3	9	2	36.0	28.0
*2	2	0	35.6	-70.6	-6	0	6	40.7	47.0	0	2	6	43.2	-36.7	1	9	2	21.3	18.2
2	4	0	6.0	-6.7	-4	0	6	15.1	14.5	0	2	7	10.6	-10.2	-3	9	2	28.2	23.5
2	6	0	8.3	5.1	-2	0	6	45.9	44.4	0	2	8	47.1	-46.4	-8	0	2	25.8	17.6
2	8	0	66.9	-60.1	0	0	6	53.7	62.1	0	2	9	9.6	-8.9	-1	9	2	10.1	7.0
2	10	0	21.5	18.0	2	0	6	56.4	63.3	0	2	10	15.8	-13.6	-2	8	2	11.0	-14.5
2	12	0	14.4	-12.8	4	0	6	43.9	45.6	0	4	2	37.5	-35.9	-2	10	2	37.4	36.0
2	14	0	29.0	-20.8	-8	0	8	30.2	36.8	0	4	3	22.4	23.0	-4	2	2	58.7	-59.7
2	16	0	21.8	16.2	-6	0	8	<12.6	-12.5	0	4	4	24.6	19.8	5	15	0	< 2.4	-1.5
2	18	0	7.8	-11.5	-4	0	8	45.4	49.4	0	4	5	9.7	9.8	6	12	0	< 2.3	3.7
2	20	0	1.2	-3.1	-2	0	8	33.6	38.2	0	4	6	13.0	10.0	6	14	0	< 2.4	-6.9
3	1	0	49.9	-55.7	0	0	8	58.7	63.5	0	4	7	17.3	17.0	6	16	0	< 2.3	9.6
3	3	0	71.3	75.7	2	0	8	51.9	58.1	0	4	8	18.3	-19.2	6	18	0	< 2.1	-4.1
3	5	0	67.9	-72.6	4	0	8	19.4	20.6	0	4	9	15.6	17.8	7	13	0	< 2.4	1.4
3	7	0	7.5	-8.6	-6	0	10	25.6	21.3	0	4	10	8.7	8.2	7	15	0	< 2.3	-4.1
3	9	0	10.7	10.0	-4	0	10	19.4	16.3	0	6	2	23.2	23.6	7	17	0	< 2.1	-4.9
3	11	0	35.1	-31.7	-2	0	10	24.3	21.9	0	6	3	2.1	2.0	8	6	0	< 2.0	0.2
3	13	0	12.9	7.2	0	0	10	57.9	56.6	0	6	4	27.3	21.4	8	10	0	< 2.3	3.1
3	15	0	5.0	-5.5	0	0	4	48.2	49.8	0	6	5	10.7	-11.8	8	12	0	< 2.4	-3.9
3	17	0	1.1	-5.5	0	0	2	34.8	45.1	0	6	6	37.3	34.6	8	16	0	< 2.2	5.2
3	19	0	5.3	5.0	7	1	1	20.8	-18.1	0	6	7	8.6	-9.6	8	18	0	< 1.8	-4.0
3	21	0	5.7	-6.5	4	8	1	8.4	-7.4	0	6	8	31.1	31.2	9	1	0	< 2.0	-1.7
4	2	0	46.6	-45.0	-1	5	1	19.4	-15.1	0	6	9	8.4	-8.0	9	7	0	< 2.2	3.2
4	4	0	3.7	-5.2	3	5	1	9.3	8.6	0	6	10	39.1	38.3	9	9	0	< 2.3	1.9
4	6	0	35.5	33.4	5	1	1	34.0	-42.9	0	8	2	60.9	-62.1	9	13	0	< 2.3	5.9
4	8	0	42.3	-35.4	3	1	1	19.3	-21.2	0	8	3	6.3	6.3	9	15	0	< 2.2	-2.1
4	10	0	16.5	14.7	1	1	1	10.1	-11.6	0	8	4	42.2	-39.5	9	17	0	< 1.8	-1.9
4	12	0	0.7	2.4	-1	1	1	19.3	19.6	0	8	5	3.2	-4.1	10	8	0	< 2.3	1.9
4	14	0	8.9	-11.3	-3	1	1	14.9	15.9	0	8	6	34.0	-30.0	10	12	0	< 2.3	5.7
4	16	0	7.9	11.0	-5	1	1	35.2	42.2	0	8	7	< 2.0	-0.1	10	14	0	< 2.2	0.1
4	18	0	4.9	-5.6	-7	1	1	29.1	31.5	0	8	8	37.9	-36.7	10	16	0	< 1.9	5.2
4	20	0	1.0	0.0	6	2	1	22.5	22.0	0	10	0	36.4	31.4	11	5	0	< 2.3	0.8
5	1	0	31.5	31.5	4	2	1	5.8	6.4	0	10	2	11.0	10.6	11	7	0	< 2.4	3.3
5	3	0	63.2	64.0	2	2	1	19.0	20.2	0	10	3	11.0	10.2	11	9	0	< 2.4	6.4
5	5	0	7.6	-4.9	0	2	1	12.3	-14.3	0	10	4	33.1	32.9	11	11	0	< 2.3	-1.5
5	7	0	45.8	40.2	-2	2	1	24.3	-24.1	0	10	5	2.2	2.4	11	13	0	< 2.2	2.2
5	9	0	24.8	19.3	-4	2	1	35.0	-39.9	0	2	11	13.8	-14.7	11	15	0	< 1.8	2.6
5	11	0	10.8	-8.2	-6	2	1	16.8	-16.4	0	4	11	14.9	13.9	12	10	0	< 2.3	-5.5
5	13	0	36.5	27.1	7	3	1	15.7	12.3	-1	5	2	52.7	-57.1	12	12	0	< 2.1	-2.9
5	17	0	7.5	-2.7	5	3	1	< 4.4	3.4	-6	0	2	38.0	37.3	12	14	0	< 1.8	-2.6
5	19	0	10.0	11.8	3	3	1	8.2	8.6	7	1	2	19.1	-15.0	12	16	0	< 1.3	-1.3
6	2	0	14.9	-15.6	1	3	1	7.7	-8.1	5	1	2	49.2	-48.5	13	13	0	< 1.7	-0.9
6	4	0	7.5	5.3	-1	3	1	15.8	-14.5	3	1	2	21.1	13.9	13	11	0	< 2.0	-2.2
6	6	0	30.8	27.8	-3	3	1	17.2	-16.6	*1	1	2	47.3	-89.3	13	9	0	< 2.2	-5.7
6	8	0	19.1	-19.0	-5	3	1	19.5	-19.7	-1	1	2	27.0	-25.6	13	7	0	< 2.3	-2.8
6	10	0	10.6	13.3	-7	3	1	14.4	-13.1	-1	3	2	25.8	31.0	13	5	0	< 2.4	-2.1
7	1	0	32.3	-30.8	6	4	1	35.4	-36.2	-1	7	2	35.0	35.8	13	3	0	< 2.4	-7.8
7	3	0	12.9	12.9	4	4	1	21.0	-23.7	6	2	2	41.5	-36.2	13	1	0	< 2.4	-1.4
7	5	0	42.5	-38.2	2	4	1	21.6	-23.0	4	2	2	37.0	-45.3	14	0	0	< 2.3	0.4
7	7	0	13.0	-11.1	0	4	1	10.3	-9.3	2	2	2	46.6	-61.0	14	2	0	< 2.3	2.8
7	9	0	1.9	-0.5	-2	4	1	20.5	22.6	-2	2	2	11.0	-14.1	14	8	0	< 2.1	0.9
7	11	0	26.1	-20.2	-4	4	1	28.4	29.3	*-2	6	2	60.9	86.2	14	10	0	< 1.9	-1.9
8	0	0	10.1	8.1	-6	4	1	22.2	20.1	* 3	3	2	58.9	83.8	14	12	0	< 1.6	2.1
8	2	0	22.3	-20.5	5	5	1	10.2	9.8	* 1	3	2	58.8	94.0	15	1	0	< 2.2	5.2
8	4	0	6.8	-7.5	1	5	1	12.1	-10.9	-3	1	2	41.3	-53.2	15	3	0	< 2.1	5.1
8	6	0	24.3	-21.0	-3	5	1	< 4.1	2.0	-3	3	2	58.6	75.5	15	5	0	< 2.1	6.8
8	14	0	3.9	-5.0	-5	5	1	36.5	-29.4	-5	3	2	16.9	17.0	15	7	0	< 1.9	-0.9
9	3	0	6.7	11.4	-7	5	1	9.3	-7.7	6	4	2	10.8	-5.8	15	9	0	< 1.7	4.2
9	5	0	6.6	-9.3	6	6	1	8.3	8.7	-7	3	2	48.7	44.7	16	0	0	< 1.9	-3.5
9	11	0	5.0	-6.8	4	6	1	14.9	15.1	7	3	2	33.0	29.5	16	2	0	< 1.9	8.0
10	0	0	28.5	25.5	2	6	1	7.4	8.6	5	3	2	9.7	13.8	16	4	0	< 1.8	3.9
10	2	0	8.7	9.5	0	6	1	14.8	-15.6	4	4	2	8.8	-6.1	14	6	0	< 2.2	0.2
10	4	0	12.8	12.2	-2	6	1	6.6	-5.5	2	4	2	11.0	-7.9	14	4	0	< 2.3	0.3
10	6	0	19.1	16.2	-4	6	1	22.4	-26.1	-2	4	2	34.5	33.6	16	6	0	< 1.7	-3.1
10	10	0	2.2	8.7	-6	6	1	19.4	-25.0	-4	4	2	12.2	-9.8	17	1	0	< 1.6	0.5
11	1	0	3.6	9.3	5	7	1	32.9	-32.4	-6	4	2	19.3	-10.6	17	3	0	< 1.5	-8.3
11	3	0	8.2	12.5	3	7	1	5.9	-4.7	5	5	2	60.3	-56.1	17	5	0	< 1.4	1.5
12	0	0	3.2	-5.4	1	7	1	14.4	-13.6	3	5	2	15.0	-18.4	18	0	0	< 1.0	-3.8
12	2	0	5.0	-7.5	-1	7	1	8.3	8.0	* 1	5	2	56.3	-81.7					
12	4	0	3.3	-8.4	-3	7	1	22.0	18.4	-5	1	2	44.0	-44.1					

* Unreliable

CHAPTER 6: DISCUSSION

The refinement of these structures has shown that the basic structure of α and β-$Cu_2P_2O_7$ is similar to the other members of the "transition metal ion" pyrophosphates. The cations are found in an irregular octahedral environment. In the β phase the major distortion of this octahedra from regularity consists of an elongation of the two Cu-O bonds related by the two fold rotation and lying nearly in the a-c plane. The two remaining unique Cu-O limits by rotations about the b axis, are displaced from ideality in opposite directions. The long Cu-O bonds lie approximately in the x direction. These octahedra share edges to form a pseudo-hexagonal network extending in the x-y plane. Adjacent sheets of these octahedra are joined by the pyrophosphate groups whose geometry has been described in the Introduction. The detailed comparison of the bonds and angles of the $P_2O_7^{4-}$ ion will be made after we have discussed the space groups.

Some ambiguity exists in the choice of space groups for the phases occurring within this series. For the β forms, the symmetry pattern of the diffracted X-rays places it in the monoclinic class and the appearance of extinct reflections labelled by the Miller indices hkl, with h + k = odd, limits the space group to C m, C 2 or C 2/m. In the analogous case of thortveitite, an apparent isostructure of β-$Cu_2P_2O_7$, Zacharizsen chose the centrosymmetric possibility C 2/m. A recent careful

redetermination of the structure by Cruickshank, Lynton and Barclay (1962) has supported this choice.

Normally one resolves the space group ambiguity by refining the structure in a low symmetry space group and if the refinement leaves the atoms in the positions corresponding to the higher symmetry (within the e.s.d.'s) then it may be assumed that the higher symmetry space group is the correct one. However, if a limited amount of data is used in the refinement, or if it is not accurate enough for any of a number of reasons, then this method of choosing the proper space group might not be conclusive. In the case of thortveitite, Cruickshank et. al. found that the agreement between observed and calculated structure factors refined in each of these space groups was about equal. However, they found that the non-centrosymmetric cases, particularly C m, gave unreasonable discrepancies between sets of chemically equivalent bonds and angles in the $Si_2O_7^{4-}$ ion. Further since the agreement should be better with a lower overdeterminancy the similar agreement in the non-centrosymmetric cases does not indicate as reliable a structure since more parameters are varied.

This same ambiguity of space group exists for members of the "transition metal ion" pyrophosphate series. In the case of the Zn and Mg pyrophosphates, the crystallographic choice of C 2/m has been confirmed by electron spin resonance studies (Chambers, Datars, Calvo (1964)) and Leung Jurn Sun (1964). In these β phases only one site is seen for the paramagnetic ions and this is consistent only with the higher symmetry C 2/m. In addition, the space group of $Mn_2P_2O_7$ has been shown to be C 2/m

by use of the anomolous dispersion of Co Kα radiation by Manganese. (C. Calvo, personal communication). The β form of $Cu_2P_2O_7$ has been refined in this centrosymmetric space group, but there is no evidence to substantiate this choice, other than the fact that the β forms of the other members of the series possess this space group.

The space group C 2/m implies that the $P_2O_7^{4-}$ ion possesses a center of symmetry at the central oxygen and thus the P-O-P angle is 180°. However, this space group could also be consistent with a strong vibration of the central oxygen atom perpendicular to the P-P vector or a completely ramdom arrangement of bent P-O-P groups between two centrosymmetrically related positions. That is, it is only necessary for the time averaged or the space averaged position of the central oxygen atom to be centrosymmetric. In the space group C 2/m the cations are on a two fold axis and are related by the mirror plane.

The intensity of the reflections common to both the α and β phases were similar and the low angle reflections characteristic of the α phase were weak, indicating that the structures differed by small atomic displacements. Thus the atomic coordinates used to refine the α-$Cu_2P_2O_7$ structure were generated from those of the β structure. Also the space group of the α structure should be derivable from that of the β structure, differing by a loss of one or more of the symmetry operations of the space group C 2/m. The space group of α-$Cu_2P_2O_7$, as determined by the diffraction symmetry and extinctions, is either C 2/c or C c which,

together with the doubled c axis, are subgroups of C 2/m, and further, can be generated by small displacements of the atoms in the β structure.

Landau and Lifshitz (1960) have shown that in the case of a second order phase transition, the less symmetric phase must have symmetry elements which form a subgroup of those of the more symmetric phase. Then the more symmetric phase must contain all the symmetry operators of the less symmetric phase. The exact nature of the phase transition in $Cu_2P_2O_7$ is not known, but the treatment of Landau and Lifshitz probably applies in this case. The α form of $Cu_2P_2O_7$ has a c glide plane and thus the space group of the β form must be either C 2/m or C m. Also, if the α form has a two fold rotation axis, the β form must also contain this symmetry operator and its space group would be C 2/m. Similarly, if the β form does not have a two-fold rotation axis then the space group of the α form would necessarily be C c.

The α-$Cu_2P_2O_7$ structure has been refined in both space groups. The bond lengths found in the C 2/c space group are much more realistic. Thus the space group is probably the correct one. The final R factors were practically the same in both refinements, even though 55 parameters, including scale constants are varied in C 2/c and 103 are variable in C c. The resulting ambiguity is identical with that found by Cruickshank in the case of thortveitite as mentioned earlier. However, in both cases, the choice of space groups is not conclusive. The choice of C 2/c as the space group of α-$Cu_2P_2O_7$ may be supported but not confirmed by a negative result in a ferroelectric or pyroelectric study.

The bending of the P-O-P angle to 156° is the most significant difference between the structures of the two phases. The electron density projection on the C face for the β phase (Fig. 6) shows that the central oxygen (O_1) is elongated in the b direction. This can be interpreted as either a vibration of the central oxygen atom in this direction or a disordered displacement of the oxygen atom up or down the b axis. Since the phenomenon of X-ray diffraction is both time averaged and space averaged, it is impossible to distinguish between the effect of vibration and random disorder. The space group requires only that the time averaged or space averaged position of the central oxygen atom be at the cell origin.

The transition from the α to the β phase is presumably associated with enhanced thermal motion of the central oxygen atom. Any vibration of the central oxygen atom must be anharmonic since the potential well has two minima.

The bond lengths and interatomic angles of the two phases of $Cu_2P_2O_7$ are compared in Table 12. In the α form, assuming the space group is C 2/c, the central oxygen atom is situated in alternate positions at 0.40A above and below the y = 0 plane, related by the c glide plane. The phosphorus atoms are displaced by 0.07A from the glide plane. The O_{31}-P-O_{32} angle has increased by 6° and the O_{31}-P-O_1 and O_{32}-P-O_1 angles are now different by 6°. The change results from the displacement of the central oxygen atom whose effect is partially compensated for by a twisting

of the PO_4^{3-} group to maintain nearly tetrahedral symmetry among the terminal oxygen atoms, consistent with the new direction assumed by the P-O(P) bond. Other changes in the molecular geometry of the $P_2O_7^{4-}$ ion are not greater than the experimental errors.

The two fold rotation axis of the β phase through the Cu^{++} ion is lost below the transition. In the space group C 2/c, the two fold rotation axis through the central oxygen atom of the anion remains $P_2O_7^{4-}$. The Cu^{++} ions are found to be displaced 0.17A in the a-c plane from their positions in the β phase and the displacement is in the direction of the major axis of their thermal motion tensor in the β phase. The Cu^{++} environment has been altered in an unusual fashion. The long $Cu-O_3$ bonds have changed drastically in the transition to the α phase. One of these bonds has increased to 3.00A and the other has decreased to 2.30A. The former value is unusually large for a Cu-O bond. The four remaining Cu oxygen ligands show a greater variation in their bond lengths. That is, there has been a radial departure from the near tetragonal symmetry of the Cu^{++} site in the β phase.

It should be possible to observe changes in the optical absorption properties of $Cu_2P_2O_7$ because of the difference between the cation octahedra of the two phases.

Strangely, the partially refined structure of α-$Mg_2P_2O_7$, (C. Calvo personal communication) which has no space group ambiguity, shows Mg-O bonds

of 2.9 and 2.7A derived from a 2.16A bond length in the β phase. The remaining ten symmetry independent Mg-O bonds lie between 2.0A and 2.2A.

A better approximation to the true bond distances may be obtained by making some allowances for the detailed nature of the thermal motion. The two extreme values of the time averaged bond length arise from completely "in phase" or "out of phase" relative atomic motion of the atoms forming the bond. However, Busing and Levy (1964) have proposed more realistic limiting assumptions. At one extreme the motion of the heavier atom is completely independent of the position of the lighter atom but the lighter atom is "riding" on the heavier atom. Secondly, it is reasonable to assume that there is no correlation between the motions of the two atoms forming a bond. The P-O bonds from both phases are shown in Table 13 with corrections applied based on both of these assumptions.

Large e.s.d.'s occur in the z co-ordinates of the atoms in the $Cu_2P_2O_7$ structures, (see Table 12). Thus the bonds which lie primarily in the c direction will have the largest errors. In particular the $Cu-O_2$, $Cu-O_3$ and $P-O_2$ bonds have e.s.d.'s of approximately 0.05A. However, the bonds which lie nearly in the xy plane are relatively accurate. The error in the P-O(P) bond, ignoring discrepancies arising from thermal motion or disorder, is 0.01A. The causes of these errors are the inherent inaccuracy of the observed structure factors and the insufficient number of observed structure factors, particularly those with non-zero ℓ.

The details of the α-$Cu_2P_2O_7$ structure were given in Table 12. The related structure of α-$Mg_2P_2O_7$ and α-$Zn_2P_2O_7$ have not been fully refined, but the preliminary results show that the P-O-P angle is bend from 180° and there is nearly a two fold rotation axis through the $P_2O_7^{4-}$ of the former ion. The value of the P-O-P angle for α-$Mg_2P_2O_7$ is 144 ± 3°. The structure $Na_4P_2O_7 \cdot 10H_2O$ (MacArthur and Beavers 1957) is not isomorphic to the "transition metal ion" pyrophosphates, but the P-O-P angle is found to be 134°. There appears to be a correlation between the increase of the electropositivity of the cation and the deviation of the P-O-P angle from 180°. This could be expected since the increasing electropositivity of the cation causes increasing charge delocalization from the anion and thus a lowering of the P-O(P) bond strength.

The phase transitions which occur in the more electropositive alkaline earth pyrophosphates are of a different nature. Knowledge of the structures of these compounds will illucidate the differences in the nature of the phase transitions and will thereby lend more experimental information to the understanding of the mechanisms involved. The nature of the other phase transtions in the "transition metal ion" pyrophosphate series suggests they are also associated with the motion or disorder of the central oxygen atom of the $P_2O_7^{4-}$ group. In each member of the series, the M-O_3' bond length is longer than the other two independent bond

lengths, $M-O_2$ and $M-O_3$. However, in the case of Cu^{++} this discrepancy is much more pronounced. The difference between the length of the $Cu-O_3'$ bond and the average of the $Cu-O_2$ and the $Cu-O_3$ bond lengths is approximately 0.67A compared with 0.15A, 0.13A and 0.25A for $Mn_2P_2O_7$, $\beta-Mg_2P_2O_7$ respectively. This discrepancy is consistent with a tetragonal Jahn-Teller effect arising from the unstable degenerate ground state of Cu^{++}. (Ballhausen (1962)). The electronic state of an atom is affected by its ligands. An octahedrally coordinated atomic site has cubic symmetry which may be distorted. Under these conditions, the ground state of $3d^9$ $^2D_{5/2}$ Cu^{++} is a degenerate e_g state. Tetragonal symmetry arises when an octahedral arrangement of ligands with perfect cubic symmetry is distorted by an equal radial displacement of a pair of centrosymmetrically related ligands. Such a distortion removes the degeneracy of the ground state and the new ground state will be the configuration of lowest electronic energy arising from the former ground state. Since the difference in energy between the new ground state and the parent e_g state will be a function of the distortion, the position of the oxygen atoms will be altered from octahedral symmetry to a point were the difference is a maximum between the energy gained from the removal of the degeneracy and the total energy required to distort the cubic symmetry of the hypothetical cation site. The spectroscopic splitting tensor for Cu^{++} in $Zn_2P_2O_7:Cu^{++}$ had anticipated this effect since the component g_{zz} of the 2nd order spectroscopic splitting tensor

was found to be 2.47 ± .002 as compared to 2.09 ± .002 for the g_{xx} and g_{yy} components (C. Calvo et. al. (1964)). Also the magnetic axis corresponding to the g_{zz} component was found to be nearly parallel to the Zn^{++}-O_3 bond direction as measured by the paramagnetism of the isotropically substituted Cu^{++} ion.

The geometry of the $P_2O_7^{4-}$ ions in the four isomorphic high temperature structures is also given in Table 14. The P-O_2 bond of β-$Zn_2P_2O_7$ is short and the same bond in β-$Cu_2P_2O_7$ is relatively long, but this value is in doubt because of the effect of the large ripples from the Cu^{++} ion. The bond angles in the $P_2O_7^{4-}$ group remain remarkably consistent throughout the series, in spite of different environments in each case.

The pertinent bond lengths and bond angles of the β-$Cu_2P_2O_7$ structure are given in Table 14 with the equivalent information for the high temperature forms of $Zn_2P_2O_7$, $Mg_2P_2O_7$ and $Mn_2P_2O_7$. In the case of $Mn_2P_2O_7$, the structure factors reported by Lakaszewicz et. al., consisting of $\{ho\ell\}$ and $\{hk0\}$ data were combined with 46$\{h, h + 2\ell, \ell\}$ additional reflections measured optically from a Weissenberg film and refined by least squares analysis, allowing for anisotropic thermal motion. The coordinates obtained were used in calculating the molecular geometry of $Mn_2P_2O_7$. The atomic coordinates of β-$Mg_2P_2O_7$ and β-$Zn_2P_2O_7$ were from Calvo (a and b, 1965).

Some of the data used in these structures determinations were collected with a manual diffractometer. Instrumental methods of measuring intensities have an advantage over visual methods in that they yield a more precise value for the intensity and that they have the inherent possibility of accelerating the recording of the data. The accuracy of the counter data was compared to that measured visually by calculating the R value for this data separately. In addition this data alone was processed through 3 cycles with the least squares program. The R value thus obtained was 0.125. Since the ratio of the number of observations to the number of variables, that is the "overdeterminancy" was substantially smaller in this case, the modest improvement obtained was not significant. This implies that other effects such as extinction, absorption and perhaps inadequate treatment of the thermal or orientational disorder may be limiting the ultimate accuracy of this structure determination.

Lazarev (1964) has carried out a series of investigations of the pyrocompounds by means of infrared absorption. In particular, the spectrum of β-$Mg_2P_2O_7$ suggest that the P-O-P angle is not linear but the central oxygen atom is probably on either side of the centrosymmetric position even though the space group of β-$Mg_2P_2O_7$ requires its averaged position to be centrosymmetric. Because of the "fuzziness" of the spectroscopic lines, Lazarev postulates that the atom is vibrating slowly in a double well potential and further that the transition to the low temperature

form probably corresponds to a "freezing in" of the central oxygen atom on alternate sides of the wells. However, his results do not rule out the possibility that the transition is an order-disorder phenomenon. The non-linear P-O-P bond has been confirmed by Calvo (1965).

The electron density projections on the $\underline{y} = 0$ and $\underline{z} = 0$ planes for both phases are shown in Figures 5 to 8. The projection on the $\underline{y} = 0$ plane seems to show lack of resolution characteristic of the effects of series termination. It appears that the limited amount of data collected with CuKα radiation is not sufficient to suppress spurious peaks in the electron density projection. If the data is taken with CuKα radiation, large terms may be left out of the Fourier series used to calculate the electron density projections and "ripples" appear. This effect probably accounts for the strong negative peak on either side of the Cu^{++} atoms in the $\sigma(x,z)$ projections. The second peak in this ripple is positive and occurs in the vicinity of the O_2 atoms as may be seen from Figure 5. Because of this, the $\underline{x}$ coordinates of the O_2 atom, when refined with the $\{ho\ell\}$ data, was quite different from that obtained when refinement was carried out with the more complete $\{hk0\}$ data. In the case of the $\sigma(x, y)$ projection, the background of negative peaks is weaker. Apparently more $\{ho\ell\}$ data are necessary. This can be obtained by decreasing the wave length since the radius of the volume of reciprocal space available for sampling is inversely proportional to the wave-length

of the radiation used in the experiment. Approximately ten times more data should be available when the MoKα radiation is used. In practise, however, if MoKα radiation is used, the atomic scattering factor, together with the atomic thermal motion reduces the average intensity to below the detectable limit at $|\sin\theta| = 1$.

The $\sigma(x,y)$ projection of the β phase shows four peaks in the region of the central oxygen atom. In order to determine whether these peaks arose from scattering matter in the crystal or the inadequacy of the Debye-Waller factor in treating a strongly-vibrating or disordered atom, a difference Fourier synthesis was computed using $\{hk0\}$ reflections. The structure factors were calculated assuming that the central oxygen was situated at the origin with large thermal motion in the b direction. The difference synthesis indicated that the proposed structure had insufficient electron density in the region of the peaks farthest from the origin, but this blended gradually into a region at the origin which had too much electron density. Thus the peaks nearer the origin are spurious and probably arise from the inadequacy of the mathematical treatment. These outer peaks could arise from a bent P-O-P angle if the space group of β-$Cu_2P_2O_7$ were C 2.

The effect of absorption is to decrease the relative intensity of low angle reflections with respect to those at higher angles. Also, because of the irregular shape of the crystals used in these studies the amount of decrease varies with the crystal orientation. The effect of the

thermal motion is to increase the relative intensity of the low angle reflections. This increase is also dependent on the crystal orientation because of the anisotropy of the thermal vibrations. For nearly harmonic atomic motions, the vibrations of a given atom can be represented by an ellipsoid whose principle axes and orientation are defined in terms of the anisotropic temperature factor components, β_{ij}. Thus uncompensated absorption will cause errors in these anisotropic temperature factor components. Approximate corrections were not made to the structure factors because the exact geometry of the samples was not known.

Because of the enhanced motion of the central oxygen atom it should be noted that the values quoted in Table 14 for interatomic angles, involving this atom are not true angles because of the enhanced thermal disordering or vibration of the central atom. These angles should be taken as time or space averaged values.

The refinement of the position of the two peaks corresponding to the central oxygen atom is limited by the resolving power of X-rays. The limit of resolution by X-rays is $0.61\lambda/(2 \sin \Theta_m)$ where Θ_m is the largest Bragg angle used (James (1962)). For the case of MoKα radiation this gives 0.31A for $\Theta_m = 45^\circ$ and for CuKα radiation, 0.67A. Therefore, it will be difficult to resolve the position of two closely placed atoms.

Also all the $\underline{y}$ coordinates of the two half atoms are highly correlated and this violates one of the approximations used in the derivation of the least squares equations.

We have attempted to describe the thermal motion of the central oxygen atom by a second order tensor $\underline{\underline{B}}$ whose components are β_{ij}. The structure factor is written

$$F_H = \sum_H f_{jH} \exp(i\vec{H}\cdot\vec{r}) \exp(-\vec{H}\cdot\underline{\underline{B}}\cdot\vec{H})$$

This is a generalization of the Debye-Waller factor. In the derivation of the Debye-Waller factor, it is assumed that:-

(i) The magnitude of the atomic vibrations is small

(ii) The vibrations are harmonic

(iii) The vibrations are not coupled.

Now, in the case of the enhanced motion of the central oxygen atom, these assumptions will not necessarily be valid. In order to properly describe this motion, the above equation must be modified. Similar modification will be necessary if the atom in statistically disordered. We may gain some knowledge of the nature of these modification by the following considerations.

Let us replace the central oxygen atom by two half atoms. Their contribution to the scattering amplitude will be

$$1/2\ f_j \exp(-\vec{H}\cdot\underline{\underline{B}}\cdot\vec{H}) \exp(2\pi i\ \vec{H}\cdot(\vec{r} + \vec{\Delta r})) +$$

$$1/2\ f_j \exp(-\vec{H}\cdot\underline{\underline{B}}\cdot\vec{H}) \exp(2\pi i\ \vec{H}\cdot(\vec{r} - \vec{\Delta r}))$$

in the place of the expression for one atom of the form

$$f_j \exp(-\vec{H}\cdot\underline{\underline{B}}'\cdot\vec{H}) \exp(2\pi i\, \vec{H}\cdot\vec{r})$$

Equating these expression we find that

$$\exp(-\vec{H}\cdot\underline{\underline{B}}\cdot\vec{H}) \cos(2\pi\, \vec{H}\cdot\Delta\vec{r}) = \exp(\vec{H}\cdot\underline{\underline{B}}'\cdot\vec{H})$$

or

$$\vec{H}\cdot\underline{\underline{B}}'\cdot\vec{H} = \vec{H}\cdot\underline{\underline{B}}\cdot\vec{H} - \ln(\cos(2\pi\, \vec{H}\cdot\Delta\vec{r})$$

$\underline{\underline{B}}'$ will be adjusted by the least squares process to fit the data to this equation but if $\vec{H}\cdot\Delta\vec{r} > 1/4$, the second term is complex. This corresponds to the matrix of $\underline{\underline{B}}'$ being non-positive definite. That is,

$$|\beta_{ii}| \leqslant 0 \text{ or } \begin{vmatrix} \beta_{ii} & \beta_{ij} \\ \beta_{ji} & \beta_{jj} \end{vmatrix} \leqslant 0 \text{ or } \begin{vmatrix} \beta_{11} & \beta_{12} & \beta_{13} \\ \beta_{21} & \beta_{22} & \beta_{23} \\ \beta_{31} & \beta_{32} & \beta_{33} \end{vmatrix} \leqslant 0$$

If $\underline{\underline{B}}$ is positive definite the β_{ij} define the principle axes of an ellipsoid of vibration in reciprocal space. This reciprocal space ellipsoid is related to an ellipsoidal distribution of electrons in real space arising from the anisotropic motion of the atom. Obviously, if this motion is large the time averaged distribution of electrons in real space can no longer by described be an ellipsoid. Thus, even though we can still approximate the description of the central oxygen atom by anisotropic temperature factor components, this treatment is not adequate.

The peculiar shape of the two peaks in Figure 6 representing the central oxygen may be a result of this inadequacy. Because of this and the absorption effects, the thermal parameters in Tables 8 and 9 can only be regarded as rough indications of the magnitude of the thermal motion.

Another problem arises in the refinement of this structure because of non-positive temperature factor components. If the determinants of the matrices in the aforementioned relations are negative, the effective scattering power does not fall off as fast as it would ignoring thermal effects. However if these determinants are large and negative the effective scattering curve diverges with increasing ($\sin \theta/\lambda$), and the calculated structure factors at large values of $\sin \theta/\lambda$ become too large by several orders of magnitude. This phenomenon caused considerable difficulty in the refinement of β-$Cu_2P_2O_7$.

In Table 2 Cruickshank predicts a value of 1.58A for the P-O(P) bond length, and 1.52A for the exterior bond length for a linear P-O-P vector, and for the 120° case, these values are 1.64A and 1.51A respectively. Since Cruickshank assumed an isolated $P_2O_7^{4-}$ ion, all the external bonds were considered equivalent. The average value of the P-O bond lengths, whose deviation from the accepted value of 1.54A for a bond order of 1.5, can give a measure of delocalization of the total charge from the anion. These values are 1.552A, 1.548A, 1.541A and 1.517A for the pyrophosphate of Mn, Mg, Zn and Cu respectively. In the light of the large errors on the z parameters in the latter case, together with the difficulties involved in

the anisotropic temperature factor components, the deviation from the expected average may not be significant. This seems to indicate no large migration of charge from the anion. However, an environmental effect is clearly apparent. The I.R. spectroscopic work of Lazarev has shown that the assumption that the pyro anion is independent of its environment is not a good one since the spectrum of the central X-O-X group vibration is shifted by varying the cation.

A detailed analysis of the role of the environment must be made from a set of bonds properly corrected for thermal motion. This cannot be done until the true nature of the disordering phenomena is known.

It is evident that in order to gain a complete understanding of the mechanism of the different phase transitions of the "transition metal ion" pyrophosphates, further investigation is required of the structures of the low temperature and intermediate forms. Also additional knowledge of the e.s.r. spectra, the specific heats and magnetic properties of these compounds will be most useful.

TABLE 12

Comparison of the Molecular Geometry of α and β $Cu_2P_2O_7$

(a) α Bond Designation	α-$Cu_2P_2O_7$ Bond Length	β-$Cu_2P_2O_7$ Bond Length
$P-O_1$	1.588	(1.532)
$P-O_2$	1.575	(1.577)
$P-O_{31}$	1.513	-----
$P-O_{32}$	1.515	(1.471)
$Cu-O_{2a}$	1.960	-----
$Cu-O_{2b}$	1.981	(1.947)
$Cu-O_{31a}$	1.922	-----
$Cu-O_{32a}$	1.890	(1.953)
$Cu-O_{31b}$	2.303	-----
$Cu-O_{32b}$	3.002	(2.616)

TABLE 12

(b) Angles (°)

	α-$Cu_2P_2O_7$	β-$Cu_2P_2O_7$
$P-O_1-P$	156.4	(180.0)
O_1-P-O_2	104.3	(103.7)
O_1-P-O_{31}	103.8	-----
O_1-P-O_{32}	110.0	(107.7)
O_2-P-O_{31}	111.1	-----
O_2-P-O_{32}	109.6	(113.0)
$O_{31}-P-O_{32}$	116.7	(111.0)
$O_{32a}-Cu-O_{31b}$	110.0	-----
$O_{31a}-Cu-O_{32b}$	109.5	(111.0)
$O_{2a}-Cu-O_{31b}$	94.6	-----
$O_{2b}-Cu-O_{32b}$	94.8	(96.2)
$O_{2a}-Cu-O_{32a}$	76.6	-----
$O_{2b}-Cu-O_{31a}$	88.1	(84.3)

TABLE 13

Corrections for Thermal Motions Applied to $P_2O_7^{-4}$ Bond Lengths

Bond		Uncorrected	"Riding" Motions	Uncorrelated Motions
β-$Cu_2P_2O_7$	$P-O_1$	1.532	1.563	1.563
	$P-O_2$	1.577	1.578	1.590
	$P-O_3$	1.471	1.495	1.495
α-$Cu_2P_2O_7$	$P-O_1$	1.588	1.591	1.627
	$P-O_2$	1.575	1.576	1.587
	$P-O_{31}$	1.513	1.513	1.523
	$P-O_{32}$	1.515	1.515	1.526

TABLE 14

Molecular Geometry of the β Forms of the "Transition Metal Ion" Pyrophosphates

Cation	M = Mn^{++}	Mg^{++}*	Zn^{++}**	Cu^{++}
(a) Bond (A)				
$P-O_1$	1.568	1.554	1.570	1.532
$P-O_2$	1.569	1.523	1.453	1.577
$P-O_3$	1.537	1.560	1.571	1.471
$M-O_2$	2.14	2.067	2.114	1.947
$M-O_3$	2.11	2.002	1.992	1.953
$M-O_3'$	2.27	2.158	2.305	2.616
(b) Angles (°)				
O_1-P-O_2	104.8	102.5	103.5	103.7
O_1-P-O_3	108.2	107.2	108.9	107.7
O_2-P-O_3	113.0	112.8	111.9	113.0
O_3-P-O_3	109.1	113.3	110.9	111.0
$O_3'-M-O_3$	117.71			111.0
$O_3'-M-O_2$	95.3			96.2
O_3-M-O_2	80.6			84.3

* Calvo, (a) (1965)

** Calvo, (b) (1965)

Fig. 5

$\sigma(x, z)$ Electron Density Projection of β-$Cu_2P_2O_7$

Legend	Cu --	⊗
	P --	⊙
	O_1 --	X
	O_2 --	+
	O_3 --	•

The contours defining the Cu atom are drawn at 1/5 the intervals of the other contours. Dashed lines represent regions of negative electron density.

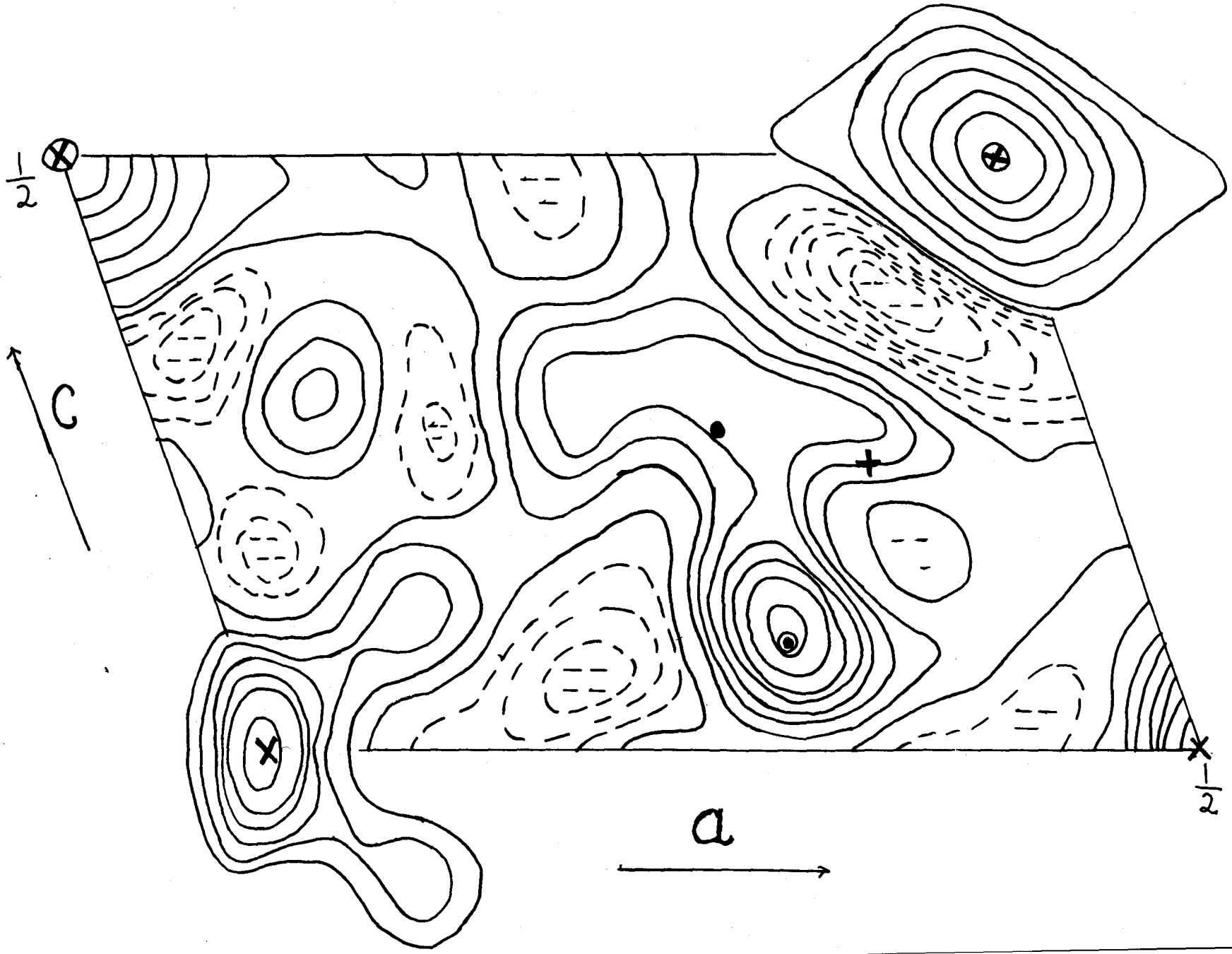
1/2
c
a
1/2

Fig. 6

$\sigma(x, y)$ Electron Density Projection of β-$Cu_2P_2O_7$

Legend	Cu --	⊗
	P --	⊙
	O_1 --	X
	O_2 --	+
	O_3 --	•

The contours defining the Cu and P atoms are drawn at 1/5 the intervals of the outer contours. Dashed lines represent regions of negative electron density.

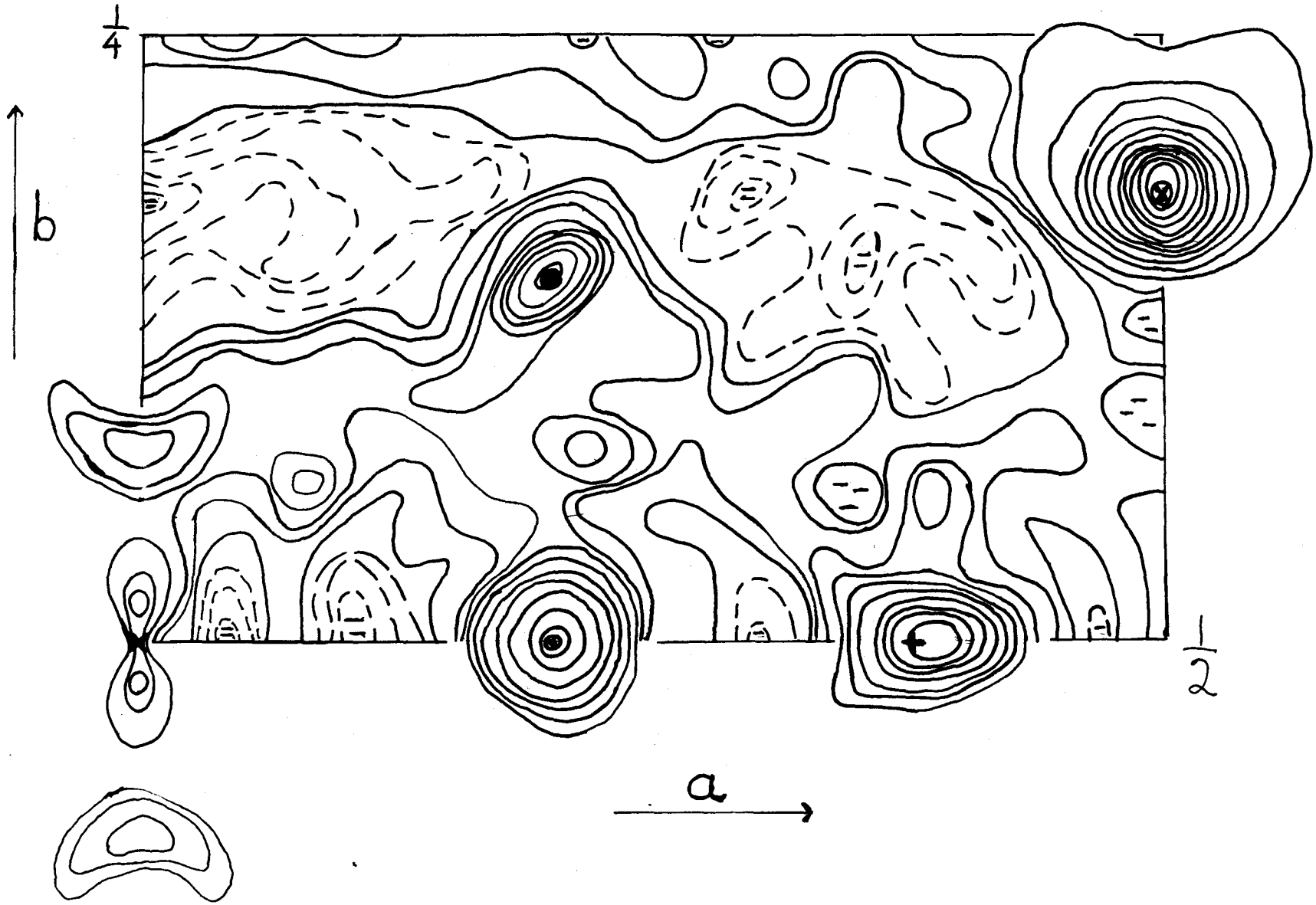
1/4
b
1/2
a

Fig. 7

$\sigma(x, z)$ Electron Density Projection of α-$Cu_2P_2O_7$

Legend	Cu --	⊗
	P --	⊙
	O_1 --	X
	O_2 --	+
	O_3 --	•

The contours defining the Cu atom are drawn at 1/5 the intervals of the other contours. Dashed lines represent regions of negative electron density.

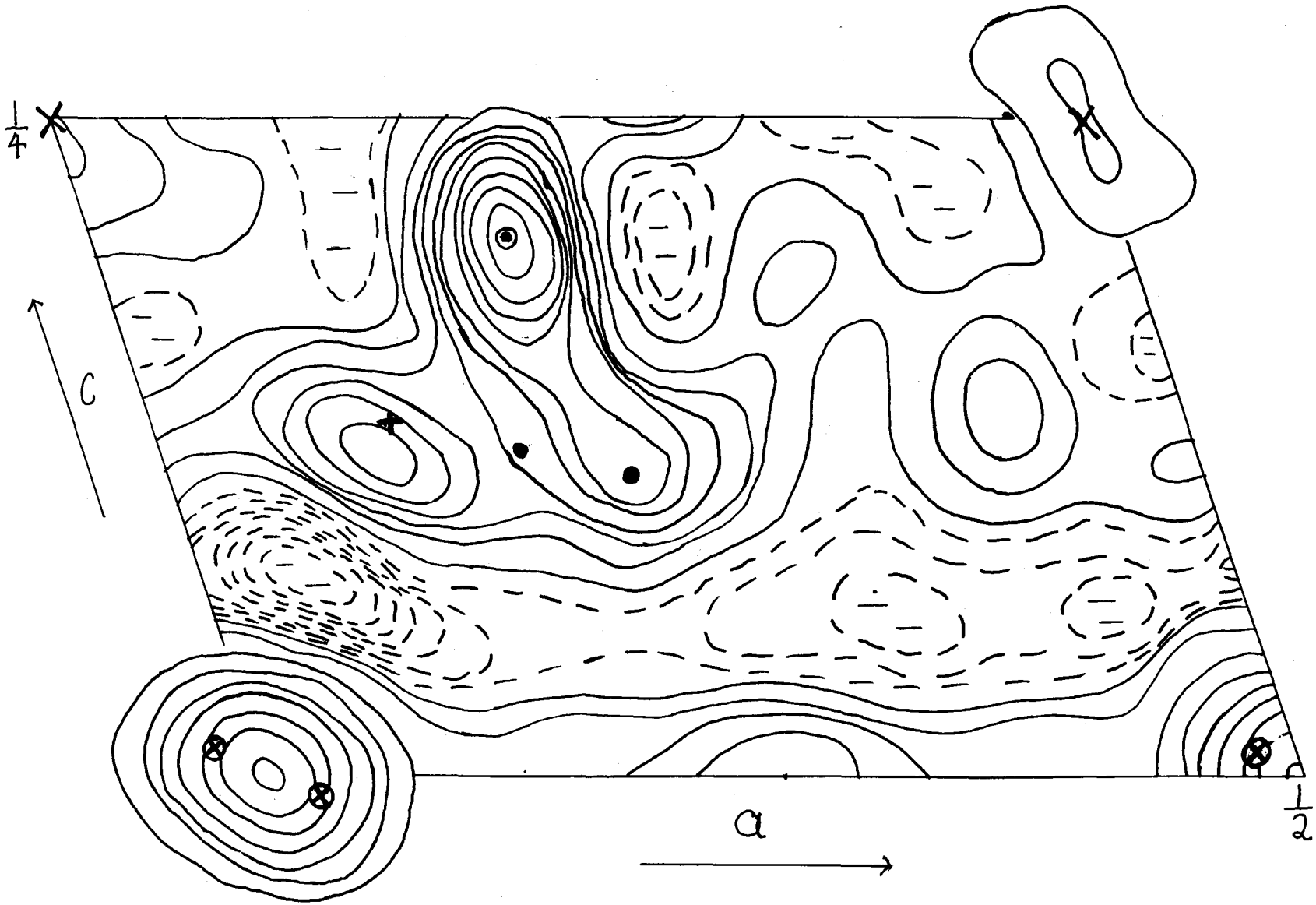
1/4
c
a
1/2

Fig. 8

$\sigma(x, y)$ Electron Density Projection of α-$Cu_2P_2O_7$

Legend	Cu --	⊗
	P --	⊙
	O_1 --	X
	O_2 --	+
	O_3 --	•

The contours defining the Cu and P atoms are drawn at 1/5 the intervals of the other contours. Dashed lines represent regions of negative electron density.

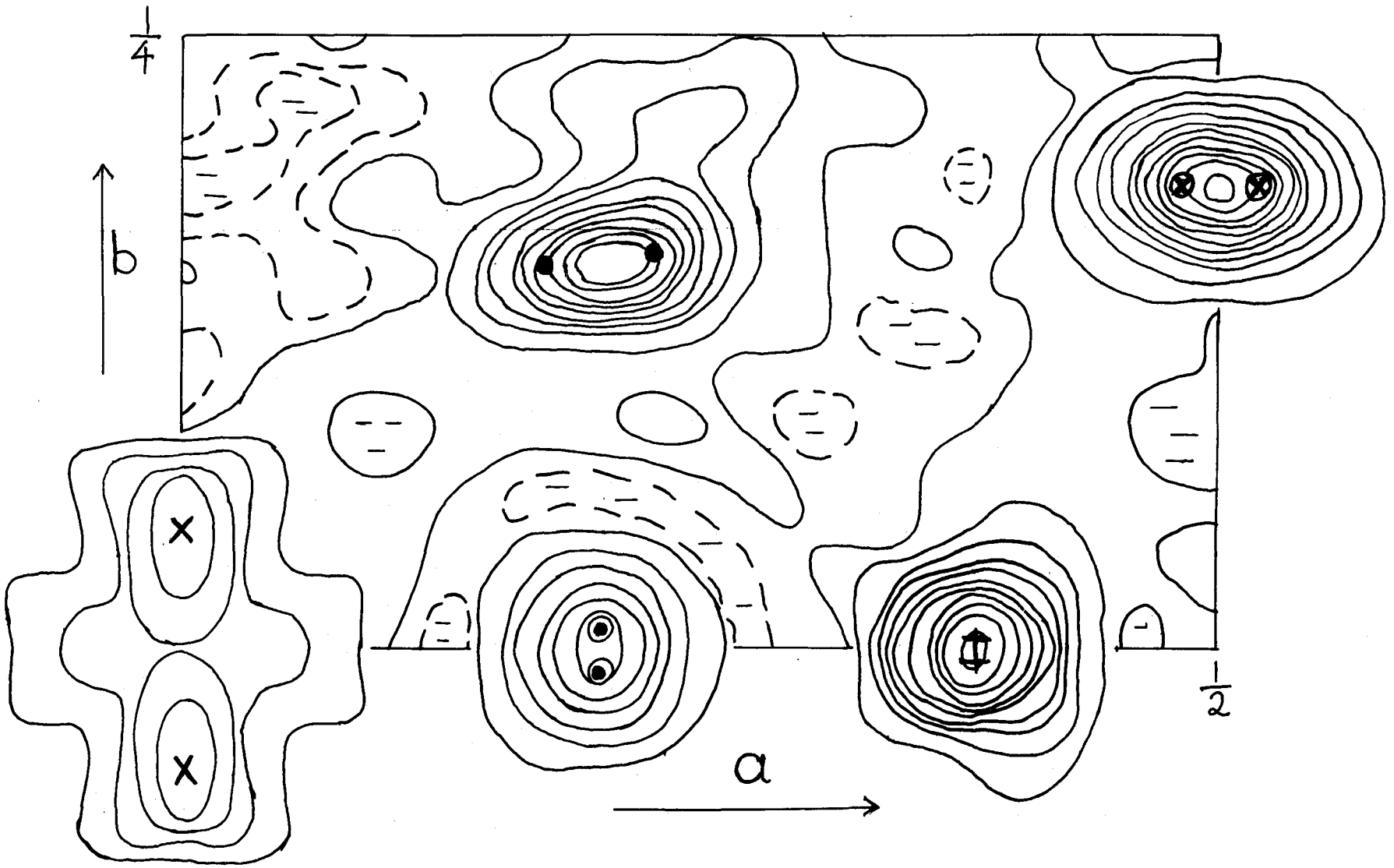
1/4
b
a
1/2

APPENDIX 1: COMPUTING FACILITIES

At the beginning of this research, a Bendix G-15 computer was available. This computer had the disadvantages that it was very slow and had a very small memory. This made it necessary to perform most calculations in steps, storing the intermediate information on paper tape. During the summer of 1963, an IBM 1620 Model I computer became available. This computer provided a larger memory and a faster rate of calculation. The size of the memory and speed were not sufficient for a useful crystallographic least squares calculation however, and a Fourier series calculation was limited to grids containing 30 by 30 points for the entire unit cell. In January 1964, an IBM 7040 was installed. This computer was much faster and contained a much larger memory than those previously available. Crystallographic least squares calculations become feasible on this machine and Fourier series calculations could be done in grids containing up to 120 x 120 points.

Also the fast access auxiliary memory proved to be very useful for crystallographic computations which involves the processing of a large amount of data. The following is a list of programs used in this research.

1. DP-10B written by Dr. I. D. Brown, Dr. B. Torrie and J. Stephens for the G-15. This program calculates, for each reflection entered, sin θ/λ and the appropriate atomic scattering factors.

2. F-10 written by Dr. I. D. Brown and Dr. B. Torrie for the G-15. This program calculates two dimensional Fourier series for any centrosymmetric space group.

3. SF-10 written by Dr. I. D. Brown and Dr. B. Torrie for the G-15. This program calculates structure factors using DP-10B output.

4. LP-X written by B. Robertson for the G-15. This program calculates Lorentz-polarization corrections to the measured intensities for three dimensional Weissenberg data.

5. DP-20 written by J. Stephens and J. Rutherford for the 1620. This program calculates three dimensional Weissenberg Lorentz-polarization corrections to all reflections supplied.

6. DP-30 written by J. Stephens and J. Rutherford for the 1620. This program calculates three dimensional precession Lorentz-polarization corrections to all refections supplied.

7. F-20-30 written by J. Brandon and Dr. I. D. Brown for the 1620. This program calculates three dimensional Fourier series at 30ths of a unit cell.

8. SF-20 written by B. Robertson for the 1620. This program calculates structure factors for centrosymmetric space groups with individual temperature factors. An R factor is also given.

9. SF-30 written by B. Robertson for the 1620. This program calculates structure factors for non-centrosymmetric space groups with individual temperature factors. An R factor is also given.

10. SP-20 written by B. Robertson for the 1620. This program calculates an overall temperature factor and scale constant for any block of data entered.

11. DP-IV written by J. Stephens and J. Rutherford for the 7040. This program calculates Weissenberg and Precession Lorentz-polarization corrections for three dimensional data, and gives Fo_H for any Io_H entered.

12. LPC written by A. K. Das and Dr. I. D. Brown for the 7040. This program calculates precession Lorentz-polarization corrections for three dimensional data with random orientation of the reciprocal axis on the film.

13. F-IV-2 written by J. Rutherford for the 7040. This program calculates two and three dimensional Fourier series of Patterson functions, electron density distributions and difference synthesis at integral fractions of 120ths of a unit cell edge.

14. BAT written by Dr. I. D. Brown for the 7040. This program calculates molecular geometry including bond lengths, interatomic angles and direction cosines of the principle axis of the ellipsoid of vibration of individual atoms.

15. SAC written by B. Robertson for the 7040. This program calculates structure factors in centrosymmetric and non-centrosymmetric space groups with individual isotropic temperature factors. The program also calculates an overall temperature factor and scale constant which are applied to the data. A final R factor is also given.

16. DIC written by B. Robertson for the 7040. This program calculates corrections for dead-time, filters and background for data obtained from the diffractometer. e.s.d.'s are also given for the data.

17. DESLID written by B. Robertson for the 7040. This program compares the Debye-Scherrer line intensity and position for the purposes of line identification.

18. DESLS written by B. Robertson for the 7040. This program refines the reciprocal lattice cell parameters from observed d spacings by non-linear least squares for any Bravais lattice system.

19. MACLS modified from a program, ORFLS, written by Busing and Levy (1962). The modifications for the 7040 were carried out by Dr. I. D. Brown, F. Hainsworth, J. Stephens and B. Robertson. This program refines a crystal structure by varying the atomic co-ordinates and anisotropic temperature factor components by non-linear least squares. Up to 87 parameters may be varied.

APPENDIX 2

Generalized Non-Linear Least Squares Analysis

Let S_i^o be a member of a set of quantities which may be observed and measured. Let $S_i^c(\vec{p})$ be a member of a set of known functions of the vector $\vec{p}$ having components p_j in a given basis. Then if the S_i^o may be measured accurately and $\vec{p}$ is accurately known, $S_i^o = S_i^c(\vec{p})$ exactly for all i. However, the S_i^o cannot be measured exactly but a sufficiently large number of them may be measured such that the problem is over-determined in the sense that many more observations are available than unknown components p_j. Then to obtain the best values of the p_j under the least squares criterion, one may minimize the function R by adjusting $\vec{\Delta p}$, where R is defined by

$$R(\vec{p} + \vec{\Delta p}) = \sum_i \left| S_i^o - S_i^c(\vec{p} + \vec{\Delta p}) \right|^2 \qquad A(1)$$

In the refinement of lattice parameters S_i^o represents the square of the reciprocal lattice spacings, d_H^* as determined experimentally from

$$do_H^{*2} = \frac{4 \sin^2 (\theta o_H)}{\lambda^2} \qquad A(2)$$

where the θo_H are the observed Bragg angles. $S_i^c(\vec{p})$ represents dc_H^{*2}, the square of the calculated lattice spacing. In general $dc_H^{*2} = (ha^* + kb^* + \ell c^*)^2$ which for the monoclinic system becomes

$$dc_H^{*2} = h^2 a^{*2} + k^2 b^{*2} + \ell^2 c^{*2} + 2h\ell a^* c^* \cos\beta \qquad A(3)$$

The components of $\vec{p}$ in Equation A(1) are a^*, b^*, c^* and β^*, the reciprocal lattice parameters.

In the refinement of a crystal structure, the S_i^o and $S_i^c(\vec{p})$ represent the observed and calculated structure factors Fo_H and $Fc_H(\vec{p})$ respectively, and the phase of $Fc_H(\vec{p})$ is assigned to Fo_H. The p_j are now the co-ordinates and anisotropic temperature factor components of the atoms in the unit cell and the scale constants to be applied to the data.

A Taylor expansion is used to find $\vec{\Delta p}$, of the form

$$S_i^c(\vec{p} + \vec{\Delta p}) = S_i^c(\vec{p}) + \sum_j \frac{\partial S_i^c(\vec{p})}{\partial p_j} \vec{\Delta p}_j + O(\vec{\Delta p}_j)^2 \qquad A(4)$$

Also we define $D_i(\vec{p}) = S_i^o - S_i^c(\vec{p})$ and drop terms of order 2 and greater in $\vec{\Delta p}_j$. Then

$$R = \sum_i \left\{ D_i(\vec{p}) - \sum_j \frac{\partial S_i^c(\vec{p})}{\partial p_j} \Delta p_j \right\}^2 \qquad A(5)$$

Now to find the minimum in R, we set the variation of R with respect to Δp_j for all j equal to zero. That is,

$$\frac{\partial R}{\partial(\Delta p_k)} = 2 \sum_i \left| D_i(\vec{p}) - \sum_j \frac{\partial S_i^c(\vec{p})}{\partial p_j} \Delta p_j \right| \frac{\partial S_i^c(p)}{\partial p_k} = 0 \qquad A(6)$$

provided the p_j are independent. These equations are referred to as the "normal" equations of the least squares refinement. In matrix form this equation becomes

$$(\underline{\underline{A}})\ (\vec{\Delta p}) = (\underline{\underline{B}})$$

where

$$A_{jk} = \sum_i \frac{\partial S_i{}^c(\vec{p})}{\partial p_j} \quad \frac{\partial S_i{}^c(\vec{p})}{\partial p_k} \text{ and } B_k = \sum_i D_i(\vec{p}) \frac{\partial S_i{}^c(\vec{p})}{\partial p_k} \qquad A(7)$$

The equation is solved by determining $(\underline{\underline{A}}^{-1})$ and multiplying through on the left in order to obtain $\vec{\Delta p}$. The process is repeated until the p_j are smaller than the error in p_j for each j.

BIBLIOGRAPHY

Ballhausen, C. J., Introduction to Ligand Field Theory, McGraw Hill, New York, 193 (1962).

Baur, W. H., Acta Cryst. 9 515 (1956).

Buerger, M. J., X-ray Crystallography, John Wiley & Sons, Inc., New York (1962).

Busing, W. R., Martin, K. O. and Levy H. A., ORNL-TM-305 (1962).

Busing, W. R., and Levy, H. A., Acta Cryst. 17, 142 (1964).

Calvo, C., (a), to be published (1965).

Calvo, C., (b), to be published (1965).

Chambers, J. G., Datars, W. R. and Calvo, C., J. Chem. Phys. 41, 806 (1964).

Corbridge, D. E. C., Acta Cryst. 10, 85 (1957).

Cruickshank, D. W. J., J. Chem. Soc. 5486 (1961).

Cruickshank, D. W. J., Lynton, H. and Barclay, G. A., Acta Cryst. 15 491 (1962).

Daniels, F., Mathews, J. H., Williams, J. W., Bender, R. and Alberty, R., Experimental Physical Chemistry, McGraw Hill Company, New York 5th ed. 120 (1956).

Evans, R. D., The Atomic Nucleus, McGraw Hill Company, New York 785 (1955).

Hoffman, C. W. W. and Mooney, R. W., J. Electrochem. Soc. 107 854 (1960).

International Tables for X-ray Crystallography, Volumes I, II and III.

Kynoch Press, Birmingham, England (1952).

James, R. W., The Optical Principles of the Diffraction of X-rays, G. Bell & Sons, London, England, 5th ed. 400 (1962).

Katnack, F. L. and Hummel, F. A., J. Electrochem. Soc. 105, 125 (1955).

Ketelaar, J. A. A., Chemical Constitution, Elsevier Publishing Company, 2nd ed. 28 (1958).

Landau, L. D. and Lifshitz, E. M., Statistical Physics, Addison Wesley Publishing Company, Inc. Reading Massachusetts, 439 (1960).

Lazarev, A. N., Izv. Akad. Nauk. SSSR Otd. Khem. Nauk. 7, 1314 (1962).

Lazarev, A. N., Izv. Akad. SSSR., Ser. Khem. 235 (1964).

Lazarev, A. N., Ibid. 242.

Lazarev, A. N., and Tenisheva, T. F., Ibid. 403.

Leung, Jurn Sun, Masters Thesis, McMaster University, Hamilton, Ontario. October, 1964.

Lipson, H. and Cochran, W., The Determination of Crystal Structures. G. Bell & Sons, London, England, 278 (1953).

Lukaszewicz, K., Roczniki Chemii 35, 31 (1961).

Lukaszewicz, K. and Nagler, E., Roczniki Chemii 35, 1167 (1961).

Lukaszewicz K. and Smajkiewicz, R. 35, (1961).

MacArthur O. M. and Beavers C. A. Acta Cryst. 10 428 (1957).

Oetting, F. L. and McDonald, R. A., J. Phys. Chem. 67 2737 (1963).

Ranby, P. W., Mash, D. H. and Henderson, S. T., Brit, J., Appl. Phys., Supplement 4, 518 (1955).

Roy, R., Middlesworth, E. T. and Hummel, F. A., Am. Mineral 33 458 (1948).

Zachariasen, W. H., Theory of X-ray Diffraction in Crystals, John Wiley & Sons, New York, 3rd. ed. 103 (1951).